Enantioenriched ruthenium-tris-bipyridine complexes bearing one helical bipyridine ligand: access to fused multihelicenic systems and chiroptical redox switches

Martin Kos,[a] Rafael Rodríguez,[b] Jan Storch,[a] Jan Sýkora,[a] Elsa Caytan,[b] Marie Cordier,[b] Ivana Císařová,[c] Nicolas Vanthuyne,[d] J. A. Gareth Williams,*[e] Jaroslav Žádný,**[a] Vladimír Církva,***[a], and Jeanne Crassous,****[b]

[a]Institute of Chemical Process Fundamentals of the Czech Academy of Sciences, v. v. i., Rozvojová 135, 165 02 Prague 6, Czech Republic
[b]Univ Rennes CNRS, ISCR—UMR 6226 ScanMat – UMS 2001, 35000 Rennes, France.
[c]Department of Inorganic Chemistry, Faculty of Science, Charles University in Prague, Hlavova 2030, 128 40 Prague 2, Czech Republic
[d]Aix Marseille Université, Centrale Marseille, CNRS, iSm2, UMR 7313, Marseille, France.
[e]Department of Chemistry, Durham University, Durham, DH1 3LE, UK.

Corresponding authors: *) J. A. Gareth Williams (j.a.g.williams@durham.ac.uk), responsible for photophysical studies of ligands and complexes, **) J. Žádný (zadny@icpf.cas.cz), responsible for the synthesis of helicenes, ***) V. Církva (cirkva@icpf.cas.cz), responsible for the original idea of photocyclization of imines, ****) J. Crassous (Jeanne.crassous@univ-rennes1.fr), responsible for the synthesis of complexes, their chiroptical and spectroelectrochemical studies.

ABSTRACT

The synthesis, photophysical and chiroptical properties of novel aza[n]helicenes (**6a**-**d**, **10a**-**b**, n = 4-7) substituted with one or two 2-pyridyl groups is described. The preparation was performed via an adapted Mallory reaction using aromatic imines as precursors. The obtained novel class of helical 2,2'-bipyridine (bipy) ligands was then coordinated to $Ru(bipy)_2^{2+}$ units, thus affording the first diastereomerically and enantiomerically pure $[RuL(bipy)_2]^{2+}$ (**11a**,**c**, L = **6a**,**c**) or $[Ru_2L'(bipy)_4]^{4+}$ (**12**, L'= **10b**) complexes. The topology and stereochemistry of these novel metal-based helical architectures were studied in details, notably using X-ray crystallography. Interestingly, the coordination to ruthenium(II) enabled the preparation of fused multihelical systems incorporating aza- and ruthena-helicenes within the same scaffold. The photophysical, chiroptical and redox properties of these complexes were examined in details and efficient redox-triggered chiroptical switching activity was evidenced.

Introduction

Helicenes are a unique class of polyaromatic compounds formed by *ortho*-fused aromatic rings, that adopt an inherently chiral helical structure.[1] Generally, the enantiomers are conformationally stable and separable by chiral HPLC, if the number of aromatic rings ≥ 6, or if the "bay positions" are substituted with bulky substituents in [5]- or [4]helicenes.[2] The extended conjugation over the aromatic rings, together with helical chirality, gives rise to unique chiroptical properties such as high molar rotation, strong electronic circular dichroism (ECD), and circularly polarized luminescence (CPL).[3]

The introduction of heteroatoms such as nitrogen within the helical scaffold gives access to azahelicene derivatives with tuned electronic and optical properties.[3b] This simple modification is sufficient to trigger exceptional properties such as improved charge transport and enhanced photophysical and chiroptical properties. Azahelicenes are thus appealing in diverse applications such as chiral dopants in organic light-emitting diodes (OLEDs),[4] chiral charge transporters in organic field-effect transistors (OFETs),[5] and spin filters for spintronics.[6] Moreover, azahelicenes can be applied as efficient chiral ligands in coordination chemistry.[3b,7] In the last decade, we and others have focussed on the development of new helical architectures bearing bidentate or tridentate coordinating moieties that — upon coordination to a variety of metal ions — lead to the formation of unique structures with remarkable optical and electronic properties.[1,3,7] Interestingly, appropriate engineering of the helicene ligand framework can generate multihelicenic systems through metal ion coordination, making this strategy an alternative to tedious, more conventional organic syntheses.[7c] This approach represents an effective way to obtain materials that display circularly polarized phosphorescence for application as chiroptical switches[8] or circularly polarized OLEDs (CP-OLEDs).[9] In this context, the ubiquity and versatility of bidentate 2,2´-bipyridine (bipy) in coordination chemistry[10] renders helicenes that incorporate this unit as particularly appealing targets.

A number of synthetic strategies have been reported for the preparation of helicene-bipy ligands, leading to products summarized in **Figure 1**. The main routes are Stille-Kelly reaction of a dibromo derivative (to give **A**),[11] [2+2+2] cycloaddition of triynes (leading to **B**),[12] C-H activation of an *N*-oxide (to generate **C**),[13] and Mallory photocyclization of stilbenes (in the synthesis of **D**, **E,** and **F**).[8,14,15] The coordination chemistry of mono- and bis-helicenic bipyridine ligands (**D** and **E** respectively) and of helicene-bis-bipyridine (**F**) to Pt(II),[8] Zn(II),[14] Re(I),[15] Ru(II)[16] and Ln(III)[17] has been studied, giving access to efficient CPL-active chiral materials, chiroptical switches, and chiral single molecular magnets (SMMs).

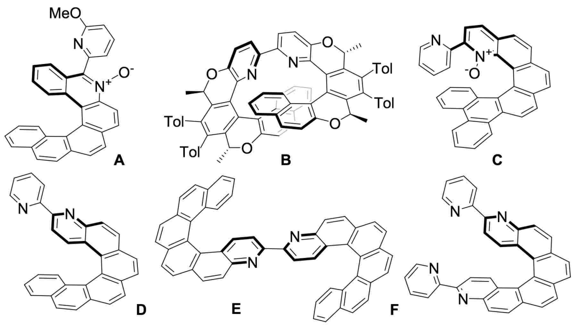

Figure 1. Examples of helicenes containing 2,2´-bipyridine units that have been reported in the literature.

Amongst the many metal complexes of bipyridines, those of ruthenium(II) have attracted remarkable attention over the last five decades. $[Ru(bipy)_3]^{2+}$ and its derivatives have an almost unique combination of properties that include high chemical stability, reversible oxidation and reduction, lowest-energy singlet and triplet excited states of metal-to-ligand charge-transfer (^{1,3}MLCT) character, excited-state reactivity, and room-temperature phosphorescence with triplet excited-state lifetimes of hundreds of nanoseconds.[18] They have found applications in various branches of chemistry such as photocatalysis, electrochemistry, and electrochemiluminescence.[18,19] Nevertheless, despite the vast development of chiral 2,2´-bipyridine ligands in homogeneous catalysis,[20] there are only limited reports on $[Ru(bipy)_3]^{2+}$ derivatives that bear centrally chiral ligands[19b] and no report of such a complex incorporating a ligand with helical chirality.

Some of the authors of the present work recently reported a novel method[21] to prepare new [n]helicenes with different numbers of aromatic units (n = 4, 5), based on a photocyclization similar to Mallory's reaction but with imines instead of olefins. Until recently, this method was still very rare[22] and preparation of helicenes by this methodology was limited to few examples formed in poor yields (2-10 %).[23] Superior reaction efficiency has recently been achieved on corannulene-based imines.[24]

Here, we report the synthesis of a novel family of helical ligands (L) bearing either one (**6a**-**d**) or two (**10a**,**b**) bipy units, via oxidative photocyclization of aromatic imines (**Figure 2**). In these ligands, the bipy moiety is grafted in a position that is different from previously reported bipyridine helicenes,[8,11-15] with a 2-pyridyl pendant at position 6 of the outer groove of a 5-azahelix. This feature offers enough room for further coordination of bulky metallic units such as $Ru(bipy)_2^{2+}$. Enantioenriched complexes of general formula $[RuL(bipy)_2]^{2+}$ (**11a**,**c**, L = **6a**,**c**) and $[Ru_2L'_2(bipy)_4]^{2+}$ (**12**, L′ = **10b**) with defined stereochemistry have thereby been prepared in this work. We show that, upon coordination, unprecedented multihelicenic fused systems[25] incorporating Ru ions are produced. In most cases, their topology and stereochemistry are dictated by the ruthenium center itself. Furthermore, taking advantage of their redox properties and strong ECD response, these complexes were characterized as redox-triggered chiroptical switches – promising materials for possible application in molecular electronic or display technologies.[26]

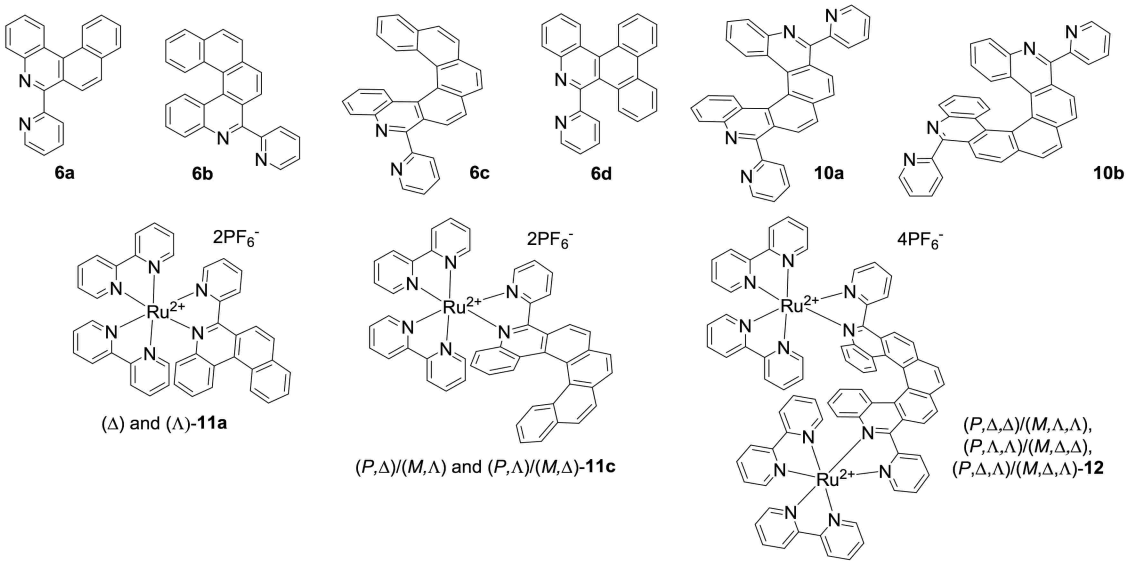

Figure 2. Targeted helical ligands incorporating bipyridine-like units (top) and their corresponding heteroleptic Ru(II) complexes, with the other coordination sites occupied by two 2,2′-bipyridines.

Results and discussion

Synthesis of helical bipyridine ligands

The efficient preparation of phenanthridines/aza[n]helicenes (n = 4, 5) bearing a pendant phenyl group *ortho* to the nitrogen atom was recently described by some of the authors, through a photocyclization reaction of aromatic imines.[21] In the current study, we extend the method to the preparation of 6-(2-pyridyl)-phenanthridine **2** (**Scheme 1**) and to helical polyaromatic hydrocarbons containing a bipy moiety (**Figure 2** and **Scheme 2**). The photochemical cyclization of imine **1** in the presence of $HBF_4.Et_2O$ and TEMPO proceeded nearly exclusively at the unsubstituted phenyl ring and gave **2** in acceptable yield (**Scheme 1**), with almost no formation of the alternative isomer **2´**. The high selectivity of the photocyclization process is due to the electron-withdrawing nature of the pyridine, enhanced by protonation under acidic conditions. The use of TEMPO protected the starting imines from undesired reduction, while molecular sieves prevented their hydrolysis.

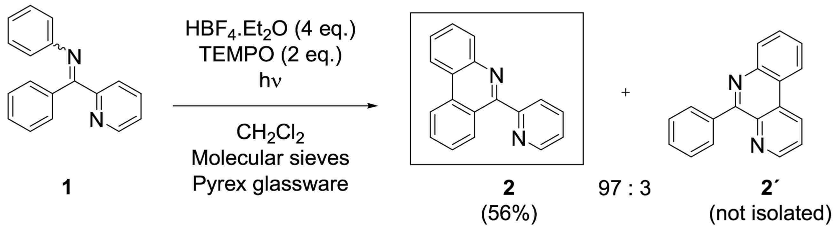

Scheme 1. Optimized conditions for the exclusive synthesis of model compound **2**.

The synthesis of more extended aromatic systems through the photocyclization of **5b** was then examined on the milligram scale and monitored by GC-MS analysis (**Table 1**). Using the conditions optimized for the preparation of phenanthridines (**Table 1**, Entry 1[21]), most of the starting material was hydrolyzed to ketone **4b**, showing the instability of **5b** in the acidic environment under irradiation. In the absence of acid (**Table 1**, Entry 2), hydrolysis of the imine was suppressed but only traces of helicene **6b** were detected in the reaction mixture. Using quartz instead of pyrex glassware led to increased conversion of **5b** to **6b**, but hydrolysis to ketone **4b** still prevailed (**Table 1**, Entry 3). The addition of Ti(O*i*Pr)$_4$ as a water scavenger was finally found to avoid hydrolysis whilst promoting almost quantitative conversion of **5b** to **6b** (**Table 1**, Entry 4). The reaction on a preparative scale under the same conditions resulted in the isolation of **6b** in 65% yield (**Scheme 2a**).

Table 1. Screening of reaction conditions for the synthesis of **6b**.

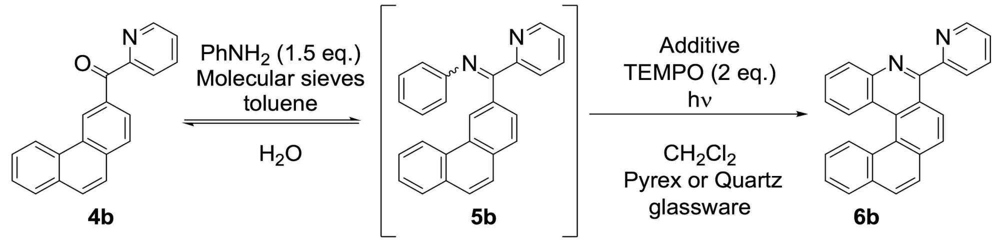

Entry	Additive, glassware	Composition of the reaction mixture after photolysis [%][(a)]		
		4b	**5b**	**6b**
1	HBF$_4$.Et$_2$O (4 eq.), Pyrex	81	0	19
2	Pyrex	2	96	2
3	Quartz	71	0	29
4	Ti(O*i*Pr)$_4$ (5 eq.), Quartz	1	3	96

(a) 2 mg of starting material; 60 min of irradiation.

These optimized conditions were utilized for the preparation of three other helicenes incorporating a bipyridyl unit: **6a**, **6c**, **6d** (**Figure 2** and **Scheme 2a**). Lithiation of aryl bromides **3a-d** and reaction with 2-cyanopyridine led to ketones **4a-d** in high yields. Their reaction with aniline gave imines **5a-d** as mixtures of *E*/*Z*-isomers, which were subsequently irradiated in the presence of Ti(O*i*Pr)$_4$ and TEMPO under inert atmosphere. Compounds **6a**,**b**,**d** with five *ortho*-fused benzene rings were isolated in up to 73% yield whilst aza[6]helicene **6c** was obtained in 48% yield. To the best of our knowledge, this is the first preparation of [n]helicene-bipy by oxidative photocyclization of imines. The product structures were unambiguously confirmed by HRMS, ^{1}H and ^{13}C NMR spectroscopy and, for **6b** and **6c**, X-ray crystallography (**Figures 3a** and **S44-S46** for ORTEP drawings). Both racemic **6b** and **6c** crystallized in the *P−1* centrosymmetric space group. 6-(2-Pyridyl)-5-aza[6]helicene **6c** exhibits a helical shape with a helicity (dihedral angle between the terminal rings) of 47°. There is a mutually *anti* arrangement of the two *N*-pyridyl rings that is typical of 2,2'-bipyridines, with a dihedral angle of 51.20°.

The same approach was further examined in the photocyclization of analogous diimines giving rise to **10a**,**b**.[27] The requisite diketones **8a**,**b** were obtained from dibromoarenes **7a**,**b** by lithiation using *t*-BuLi and subsequent reaction with 2-cyanopyridine (**Scheme 2b**). Reactions of **8a**,**b** with aniline gave diimines **9a**,**b**. The irradiation of crude **9a**,**b** in the presence of Ti(O*i*Pr)$_4$ and TEMPO led to diazahelicenes **10a**,**b** in fair yields. Their C_2 symmetry is reflected in simpler NMR spectra (full characterization is given in the SI). The structure of **10b** was also confirmed by X-ray diffraction analysis of a single crystal grown by slow diffusion of acetonitrile into a chloroform solution (**Figure 3b**). Racemic 6,13-bis-(2-pyridyl)-5,14-diaza[7]helicene **10b** crystallizes in the *P−1* space group: it exhibits a helicity of 35.06° and dihedral angles of the two trans-bipy units of 43.01-43.87°.

[n]Helicenes with n ≥ 6 possess a racemization barrier > 150 kJ mol^{-1}, which enables the (*M*)- and (*P*)-enantiomers to be isolated at room temperature.[1,28] Ligands **6c**, **10a**, and **10b**, each formed as racemic mixtures, were separated into their constituent enantiomers by semi-preparative HPLC over a Chiralpak® IE stationary phase (for details, see the SI). All enantioenriched samples were obtained with enantiomeric excesses (ee's) between 95 and 99.5% (see SI).

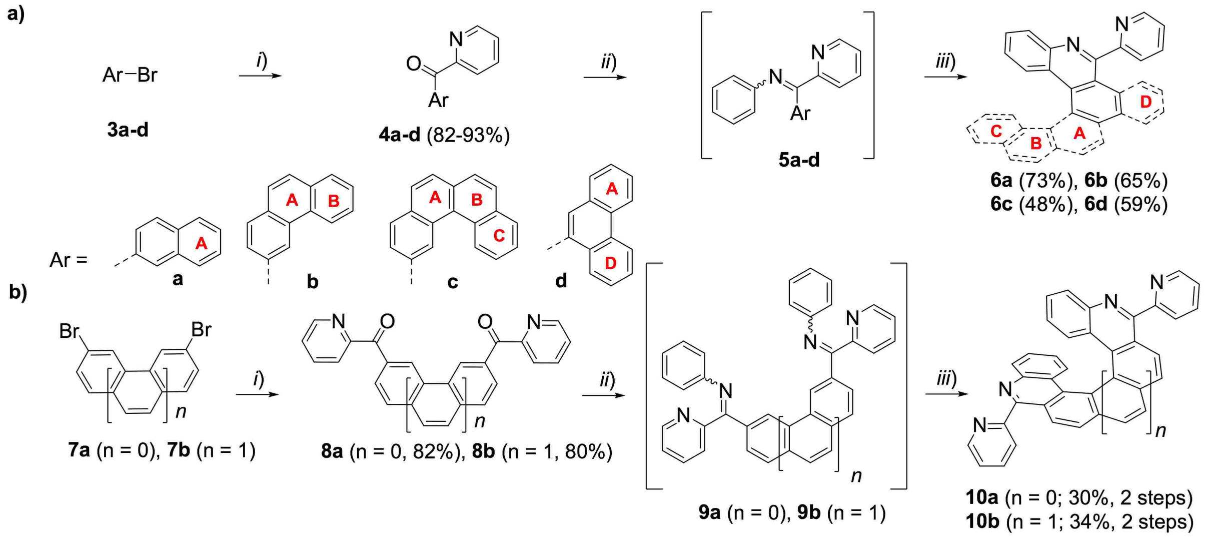

Scheme 2. Synthesis of a) bipyridine helicenes **6a**-**d** and b) diazahelicene-bis-bipyridines **10a**,**b**. *i*) *n*-BuLi, THF, −78° C, then 2-cyanopyridine then H$_2$O; *ii*) PhNH$_2$ (1.5 eq.), toluene, M.S.; *iii*) Ti(O*i*Pr)$_4$ (5 or 10 eq.), TEMPO (2 or 4 eq.), hv, CH$_2$Cl$_2$, quartz glassware.

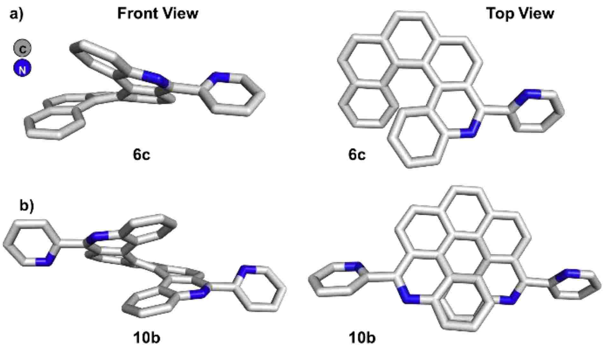

Figure 3. Single crystal x-ray diffraction structures of a) **6c** and b) **10b** (H atoms have been omitted for clarity).

Photophysical and chiroptical properties of ligands 6c and 10a,b

The helicene ligands **6c** and **10a**,**b** display broad and intense UV-visible (UV-vis) absorption spectra in the 200-400 nm range (**Figure 4a**, bottom). They are fluorescent in solution at room temperature, as observed for previously described azahelicenes.[8,15] They display slightly structured emission bands in the blue region of the spectrum (**Figure 4b**, bottom). As expected, the emission maxima increasingly red shift with increasing conjugation, with **10b** displaying the lowest energy emission. In CH_2Cl_2 solution, the structure is more pronounced, with the 0,0 vibrational component being the most intense (**Figures S51–S53**). Under these conditions, the fluorescence quantum yields are of the order of 2-7 % (10% for **6a**) and corresponding lifetimes are of the order of a few nanoseconds (**Table S1**), values that are quite typical of aza-aromatics. In a frozen glass at 77 K, the fluorescence (which is marginally blue-shifted compared to room temperature) is accompanied by structured phosphorescence bands at lower energy (**Figures S51–S53**). This spin-forbidden emission from the triplet state is characterized by very long lifetimes of around 1 second (**Table S1**).

The ECD spectra of the three pairs of enantiomers are displayed in **Figure 4a** (top part). Ligand (*P*)-**6c** shows a strong negative band at 246 nm ($\Delta\varepsilon = -260\ M^{-1}\ cm^{-1}$) and a strong positive one at 330 nm ($\Delta\varepsilon = +230\ M^{-1}\ cm^{-1}$) accompanied by a weaker positive band at 284 nm ($\Delta\varepsilon = +60\ M^{-1}\ cm^{-1}$). Ligand **10a** follows a similar pattern with much weaker signals ($\Delta\varepsilon_{max}$ □ 140 $M^{-1}\ cm^{-1}$). Qualitatively, the helical shape of the molecule is disturbed by the presence of the additional pyridyl group which may explain such a decrease, as a result of modifications of the magnetic and electric dipolar moments. The main bands in the ECD spectrum of **10b** are red-shifted by around 20 nm compared to **6c** and **10a** and of overall higher intensity. This can be classically explained by the more extended π-conjugation and different helical pitch in heptahelicenes as compared to hexahelicenes. Thus, (*P*)-**10b** displays a strong negative band at 263 nm ($\Delta\varepsilon = -220\ M^{-1}\ cm^{-1}$) accompanied by a weaker negative band at 302 nm ($\Delta\varepsilon = -90\ M^{-1}\ cm^{-1}$) and a strong positive one at 349 nm ($\Delta\varepsilon = +320\ M^{-1}\ cm^{-1}$). The polarization of the emitted light was studied by CPL spectroscopy (**Figure 4b**, top). The (*P*)- and (*M*)-enantiomeric pairs of **6c**, and **10a**,**b** display mirror-image CPL spectra with equal but opposite-sign g_{lum} values recorded around the emission maxima, ((*P*)/(*M*)-**6c**: $+4.0/-3.7\times 10^{-3}$, ((*P*)/(*M*)-**10a**: $+1.1/-1.2 \times 10^{-3}$, and ((*P*)/(*M*)-**10b**: $+5.4/-5.4 \times 10^{-3}$), in line with CPL data of previously investigated bipyridine helicenes (g_{lum} □ 10^{-3}).[8,15]

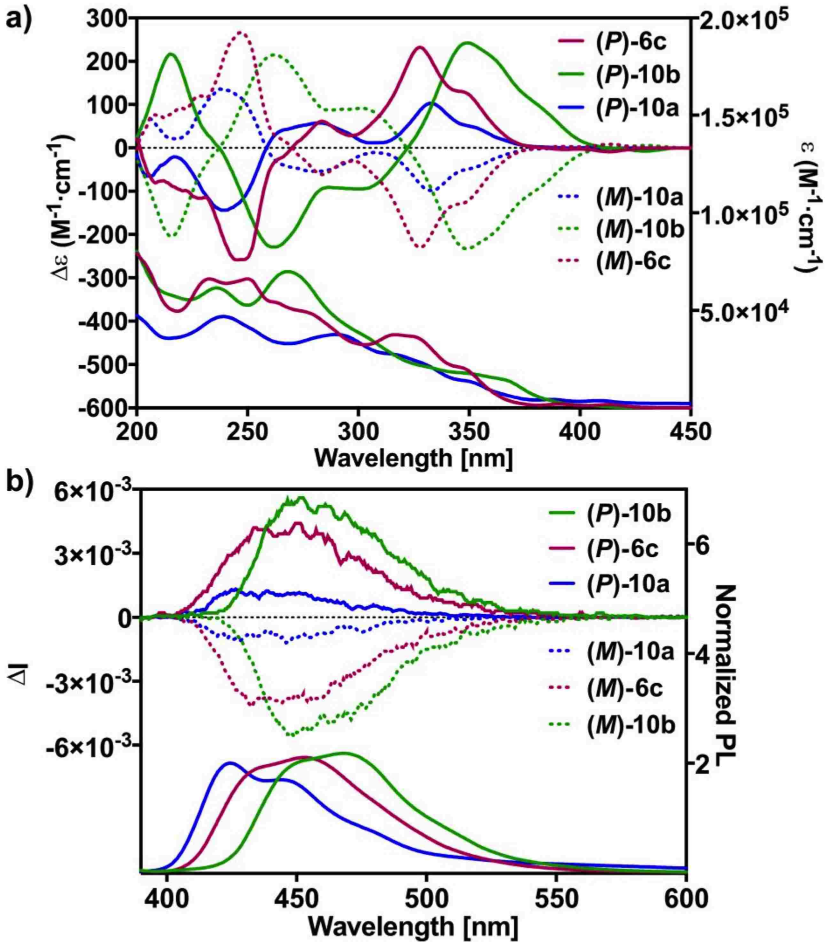

Figure 4. a) ECD (up) and UV-VIS spectra (bottom) of (*P*)/(*M*)-**6c**, **10a**, and **10b** in MeCN (~10^{-4} M) at r.t. b) Emission (bottom) and CPL (up) spectra of **6c**, **10a**, and **10b** in MeCN (~ 10^{-5} M, λ_{ex} = 360-365 nm) at r.t.

Synthesis and characterization of ruthenium complexes

The preparation of Ru(II) complexes of the $[RuL(bipy)_2]^{2+}$ form (**11a**,**c** and **12**) was achieved by directly reacting the helicene-bipy ligands L with $Ru(bipy)_2Cl_2$ in a polar solvent.[29] Such a reaction of achiral [4]helicene **6a** with racemic $Ru(bipy)_2Cl_2$, followed by metathesis of the chloride anion to hexafluorophosphate, yielded a racemic mixture of (Δ) and (Λ)-[Ru(bipy)$_2$**6a**]$(PF_6)_2$, henceforth referred to as **11a** (**Scheme 3a**). Enantioenriched (Δ)-**11a** and (Λ)-**11a** were obtained by using chirally resolved precursors (Δ)-$[Ru(bipy)_2(py)_2]$((*R*,*R*)-dbt) and (Λ)-$[Ru(bipy)_2(py)_2]$((*S*,*S*)-dbt) (dbt = *O*,*O´*-dibenzoyl-tartrate),[30a,b] in place of racemic $Ru(bipy)_2Cl_2$, followed by anion exchange with KPF_6. Due to the presence of the asymmetric bipyridine **6a**, complex **11a** has C_1 symmetry. As a result, all the signals of the atoms are chemically inequivalent in the ^1H and ^{13}C NMR spectra (see SI).

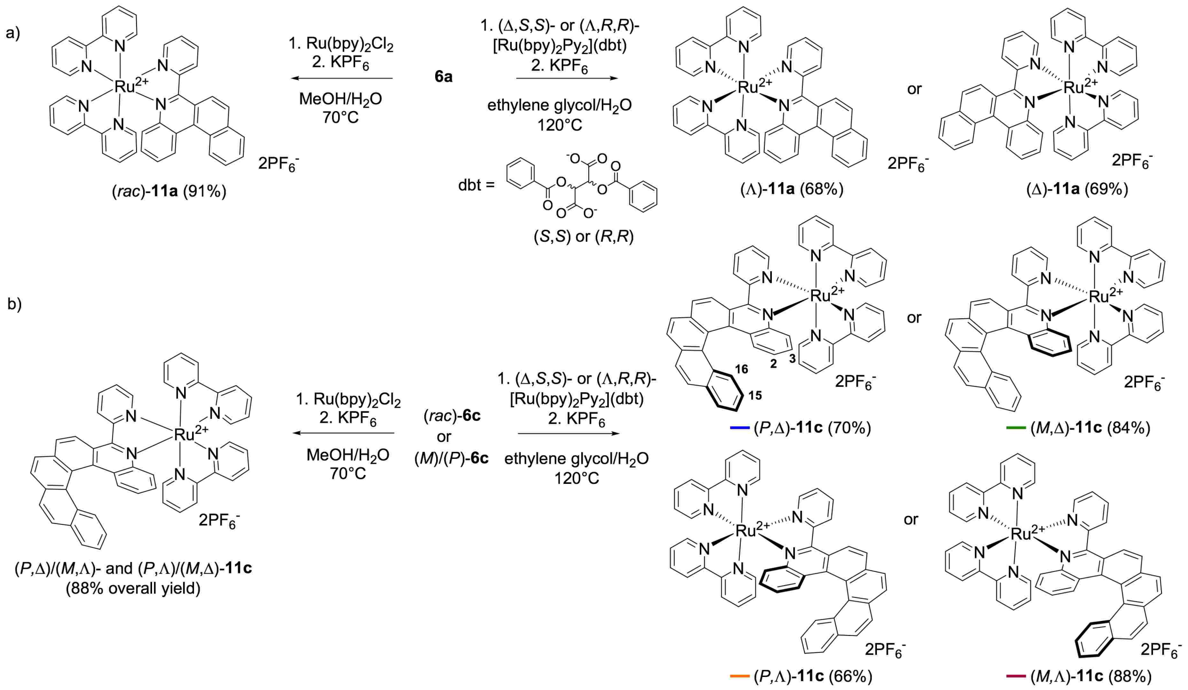

Scheme 3. Synthesis of a) racemic and enantioenriched **11a** and b) diastereomeric mixture (*P*,Δ)/(*M*,Λ)- and (*P*,Λ)/(*M*,Δ)-**11c** and of diastereo- and enantioenriched **11c**; the colors indicated correspond to those used in **Figure 7**.

The structure of **11a** was further confirmed by X-ray crystallography of a single crystal grown by slow diffusion of Et_2O into a MeCN solution of (*rac*)-**11a**. It crystallized in the *P−1* centrosymmetric space group in which both enantiomers Δ and Λ are present (**Figures 5a** and **S47**). Remarkably, upon coordination with Ru(II), the bipy helicene **6a** generates a fused metallic bis-helicenic system —one aza[4]helicene (displaying a helicity of 26.35°) and one ruthena[4]helicene (Ru[4]H in **Figure 5c**) with a helicity of 38.62°. This approach thus represents a simple, yet powerful procedure to generate metal-based multihelicenic systems. Additionally, the fixed Λ configuration at the ruthenium centre induces the *M* helix in the generated ruthena[4]helicene and the *P*-handed one in the fused aza[4]helicene (and *vice-versa*), thus demonstrating control of the helical stereochemistry by the ruthenium in the solid. However, these [4]helicenic architectures are most probably fluxional in solution.

The reaction of (*rac*)-Ru(bipy)$_2$Cl$_2$ with (*rac*)-**6c** in place of achiral **6a**, followed by Cl^- to PF_6^- metathesis, should give a diastereomeric mixture of forms of **11c** due to the presence of two stereogenic elements: helically chiral *M*/*P* helix and the Δ/Λ chirality at the metal (**Scheme 3b**). Indeed, the complicated ^{1}H NMR spectrum of **11c** after purification by column chromatography was attributed to two sets of signals (see SI, **Figure S29**). To our delight, a single crystal of the enantiomeric pair (*M*,Λ)/(*P*,Δ)-**11c** suitable for X-ray analysis was obtained by slow vapor diffusion of Et_2O into a MeCN solution (**Figures 6a** and **S48**). Comparison of the NMR spectra of crystals and mother liquor revealed an almost perfect separation of the diastereomers and also enabled the assignment of some signals to the corresponding diastereomers (See **Figures 7** and **S29**). By this comparison, it was found that (*M*,Λ)/(*P*,Δ)-**11c** was present in the originally formed mixture in a small excess of 59 : 41. It is notable that the coordination to Ru(II) provokes the formation of a ruthena[4]helicene (with a helicity of 44.35°) fused to the aza[6]helicene unit (of 54.82° helicity), in which the (*M*,Λ) unit imposes the (*M*)-Ru[4]H helix, and *vice-versa*, in the solid state. However, no conclusion can be drawn in the solution state where the ruthena[4]helicene unit is expected to be fluxional.

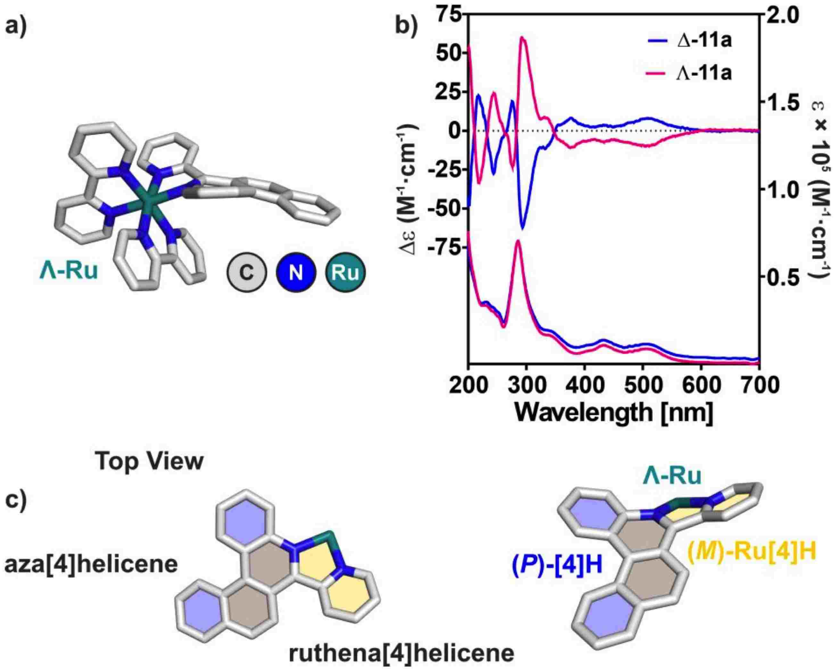

Figure 5. Single crystal x-ray diffraction structures of a) **11a** and c) selected views of the helicenic parts, PF_6^- anions and H atoms were omitted for the sake of clarity; b) UV-VIS (bottom) and ECD (up) spectra of (Δ)/(Λ)-**11a** in MeCN (□ 10^{-4} M) at r.t.

To obtain diastereo- and enantioenriched **11c**, the reaction between (*M*)/(*P*)-**6c** and resolved (Δ)-[Ru(bipy)$_2$(Py)$_2$]((*S*,*S*)-dbt)/(Λ)-[Ru(bipy)$_2$(Py)$_2$]((*R*,*R*)-dbt) precursors was conducted (see **Scheme 3b**). In all cases, the minor diastereomer was present in approximately 10% as revealed by ^{1}H NMR analysis (see SI, **Figure S34**) suggesting that the reaction did not proceed with complete stereoselectivity in the sense of Δ/Λ isomerism.

Finally, the complexation of bis-bipyridine [7]helicene **10b** to Ru(II) precursor was studied (**Scheme 4**). The reaction of (*rac*)-**10b** with 2 equivalents of (*rac*)-Ru(bipy)$_2$Cl$_2$ provided two major products which were separated by column chromatography. Both compounds were unambiguously identified by mass spectrometry as bis-ruthenium complex **12** and mono-ruthenium complex **13**. In the case of **12**, a single crystal of the (*P*,Λ,Λ)/(*M*,Δ,Δ)- enantiomeric pair was obtained by slow vapor diffusion of CHCl$_3$ into a MeCN solution of **12** (**Figure 6c**). Here again, in complex (*P*,Δ,Δ)-**12**, two fused Ru[4]H helicenes are formed. They display helicities of 26.60 and 33.62° but different (*P*) and (*M*) configurations within the same complex, thus showing no control of their chirality in the solid. In addition to (*M*,Δ,Δ)- and (*P*,Λ,Λ)- isomers, the diastereomeric mixture also contained the mixed C_1 symmetrical (Δ,Λ)-isomer (see SI, **Figure S35**). For **13**, a single crystal containing the (*P*,Λ)/(*M*,Δ)-enantiomeric pair was grown by slow vapor diffusion of Et$_2$O into a MeCN solution of **13** (see **Figure S50**). Upon coordination, a fused Ru[4]H helicene displaying a 35.55° helicity is also formed, with its (*M*) configuration controlled by the (*P*)-heptahelicene and *vice-versa*, thus showing induction of chirality in the solid state.

Diastereo- and enantioenriched complexes **12** were synthesized by the reaction of (*M*) or (*P*)-**10b** with either (Δ)-[Ru(bipy)$_2$(Py)$_2$]((*S*,*S*)-dbt) or (Λ)-[Ru(bipy)$_2$(Py)$_2$]((*R*,*R*)-dbt) precursors (**Scheme 4**).

Even though an excess of the ruthenium precursor was employed, the synthesis of the dinuclear complex **12** was always accompanied by the formation of a small amount of mono-Ru intermediate **13** (for details see SI). Both ruthenium ions in the enantioenriched forms of **12** have (Δ,Δ)- or (Λ,Λ)-configuration. As a result, all complexes possess an overall C_2 symmetry. In (*P*,Λ,Λ)/(*M*,Δ,Δ)-**12**, part of a terminal ring of the helical scaffold is strongly shielded by 2,2´-bipyridine placed in its vicinity. This is reflected in a significant change in the chemical shifts of 2-H (5.27 ppm) and 3-H (6.16 ppm), which are up to 1 ppm lower in comparison to the other enantiomeric pair (see **Figure S35**).

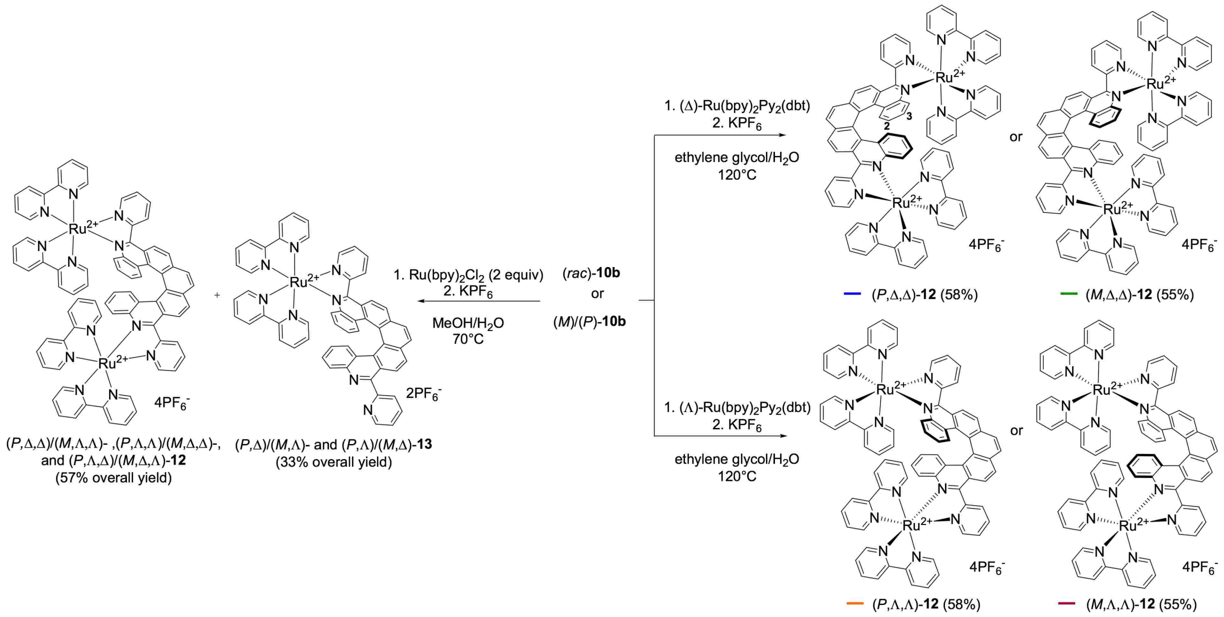

Scheme 4. Synthesis of diastereo- and enantioenriched complexes **12**, either as mixtures or as pure stereoisomers; the colours indicated correspond to those used in **Figure 6.**

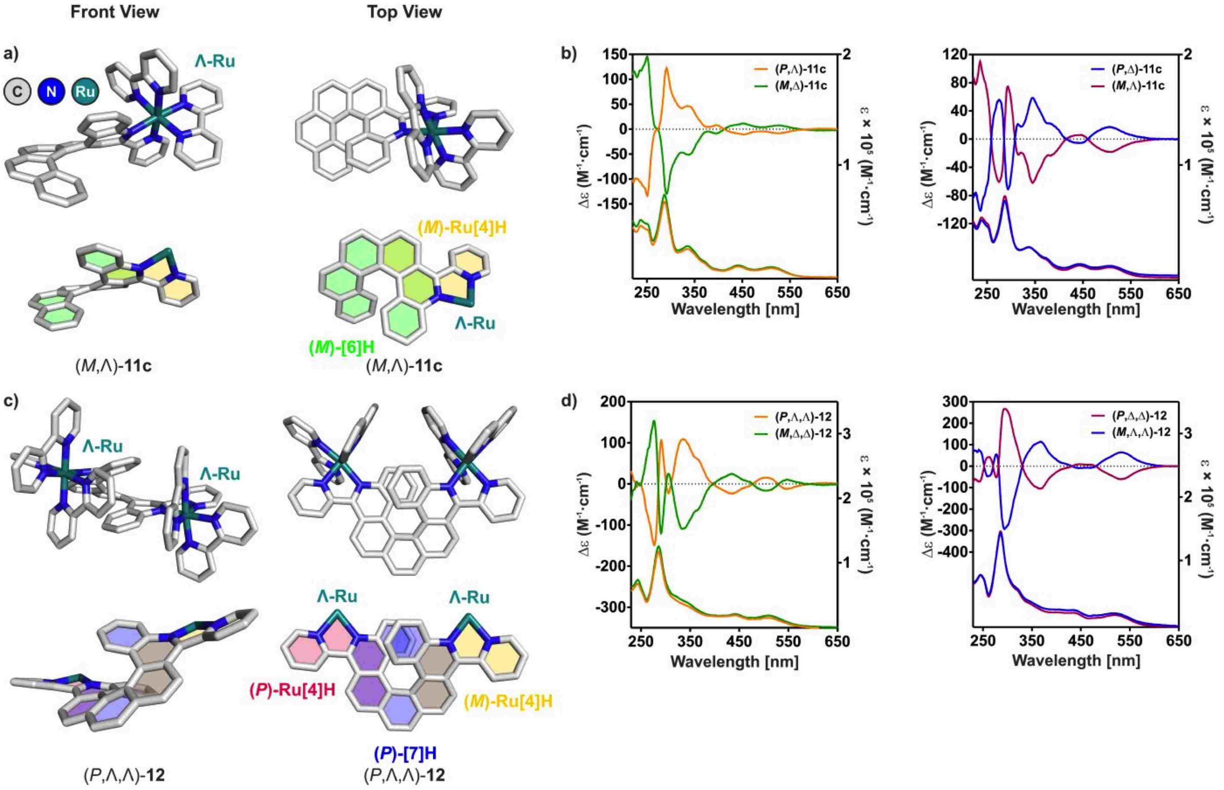

Figure 6. Single crystal x-ray diffraction structures and selected views of a) (*M*,Λ)-**11c** and c) (*P*,Λ,Λ)-**12**. PF_6^- anions and H atoms were omitted for the sake of clarity. UV-VIS (bottom) and ECD (up) spectra of b) (*P*,Λ)/(*M*,Δ)/(*P*,Δ)/(*M*,Λ)-**11c** and d) (*P*,Λ,Λ)/(*M*,Δ,Δ)/(*P*,Δ,Δ)/(*M*,Λ,Λ)-**12** in MeCN (□ 10^{-4} M) at r.t.

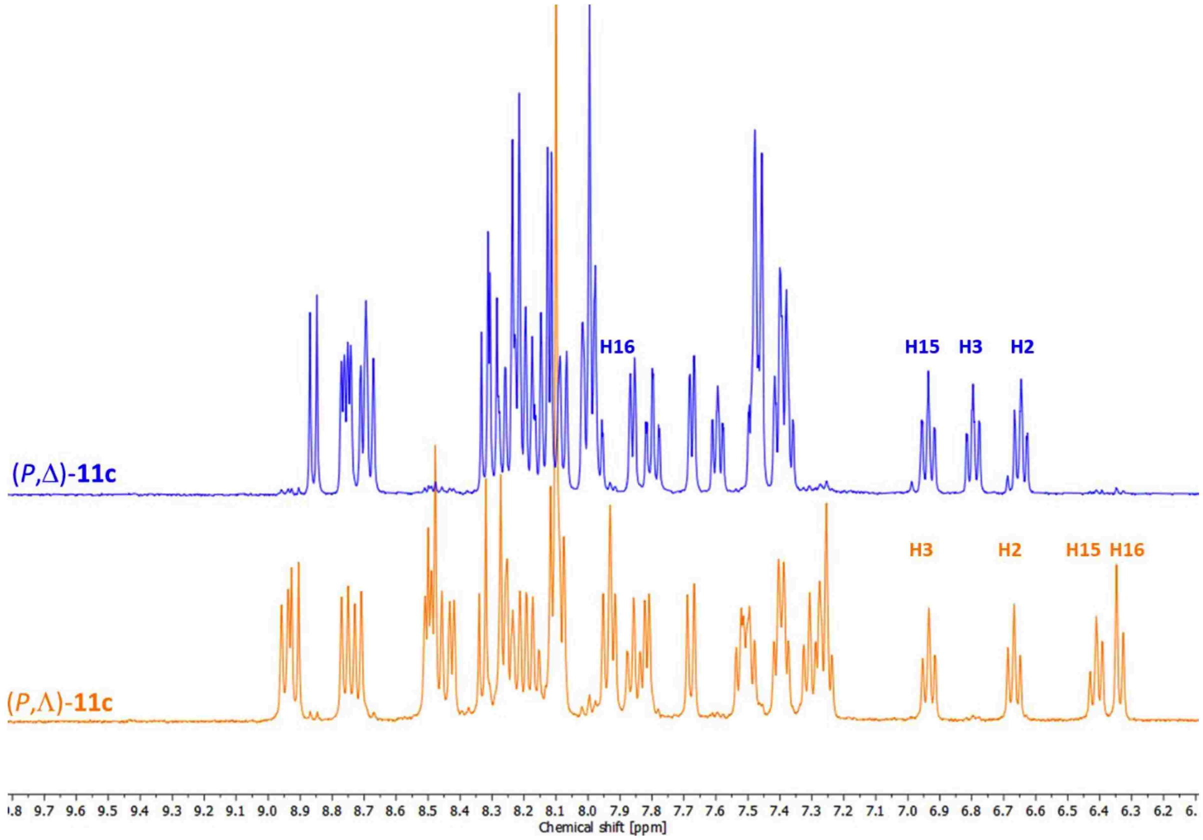

Figure 7. Comparison of ^{1}H NMR spectra of (*P*,Δ)- and (*P*,Λ)-**11c** at 400 MHz in CD_3CN at r.t. See numbering in **Scheme 3b**.

Luminescence properties of complexes 11a, 11c, and 12

Complexes **11a**, **11c**, and **12** display broad and intense UV-vis absorption spectra (**Figures 5** and **6**, bottom parts and **Figure 8**), with very similar features, notably a strong absorption band around 290 nm, and moderately intense ones around 250 and 350 nm, likely corresponding to π-π* transitions of the ligands. These bands are almost one order of magnitude stronger in the hexa- and heptahelicenic complexes **11c** and **12** than in **11a**.[18] They are accompanied by two bands of weaker intensities around 450 and 520 nm that are commonly assigned to MLCT-type transitions. Much of the intense interest in $[Ru(bipy)_3]^{2+}$ and its derivatives over the past 40 years has been driven by their attractive emission properties. $[Ru(bipy)_3]^{2+}$ is the archetypal ^{3}MLCT emitter.[18,31] The coordination as opposed to organometallic nature of the bonding, and the relative energies of orbitals, are such that the HOMO is primarily localized on the metal and the LUMO on the ligand. The ^{1,3}MLCT energies can thus be rationalized and controlled according to the nature of the ligands, often showing good correlation with the oxidation and reduction potentials.[18a,32] In heteroleptic analogs, the LUMO is typically localized largely on the ligand(s) having the lowest-energy π* orbitals associated with it. Thus, where one bipy ligand is replaced by a more conjugated analogue, a reduction in the ^{3}MLCT and ^{1}MLCT energies can be anticipated; indeed, numerous such examples have shown the expected red-shift in the emission and lowest-energy absorption bands, respectively, as a consequence.[18,31,33]

In the present series of heteroleptic complexes, such an effect is to be expected, since the extended conjugation of the helicene bipyridine ligand will serve to lower its π* orbitals. The effect is immediately clear in the absorption spectra (**Figures 5b**, **6b** and **d**, **8**, and **Table 2**), where it can be seen that the lowest-energy absorption bands are centered around 510–520 nm in each case. These values contrast with that of around 455 nm for $[Ru(bipy)_3]^{2+}$ under the same conditions, indicating a stabilization of the ^{1}MLCT state of around 2500 cm^{-1} as a result of the more extended conjugation associated with the aza-aromatic. There is, however, little difference between **11c**/**12** and **11a**, indicating that the additional aromatic rings incorporated within the helicene ligands of **11c**/**12** – remote from the quinoline moiety – have little influence in further stabilizing the LUMO compared to the parent **11a**.

All of the new complexes are found to be luminescent in solution at room temperature (**Table 2**). The emission and excitation spectra of (*M*,Δ)-**11c** and (*P*,Λ,Λ)-**12** in MeCN at 295 K are shown in **Figure 8**, together with the emission spectra in PrCN at 77 K. Corresponding spectra of the other diastereomers of **11c** and **12**, and of the parent (*rac*)-**11a**, are given in the SI (**Figures S54–S56**). The onset of the emission is around 700 nm in each case, such that most of the luminescence falls in the NIR region of the spectrum with maxima around 790 nm (**Table 2**). This is a challenging part of the spectrum for detection, being at the edge of the range for conventional visible photomultiplier tubes, yet somewhat too short wavelength for NIR detectors. Optimal results were obtained using a back-illuminated deep-depletion CCD detector (details of instrumentation are given in the SI). As in absorption, there is a large red-shift in the emission maxima relative to $[Ru(bipy)_3]^{2+}$, reflecting the stabilization of the ^{3}MLCT associated with the more extended conjugation on the ligand. Again, there is little difference between the complexes **11c**/**12** and **11a**. The emission maxima of around 780 nm compare with values of 700 and 742 nm for quinoline-containing complexes $[Ru(bipy)_2(pq)]^{2+}$ and $[Ru(bipy)_2(biq)]^{2+}$, which are perhaps the closest literature models (pq = 2-pyridylquinoline; biq = 2,2'-biquinoline).[34a] A complex featuring an azabenzannulated perylene diimide could be construed as a related example featuring the benzannulated phenanthridine moiety of the present complexes, for which λ_{max}^{em} = 780 nm, though the nature of the excited state is quite different in that case.[34b]

The luminescence quantum yields are low, of the order of 0.1% (**Table 2**). Low values are to be anticipated, given the low energy of the excited state and the fact that the energy gap law typically applies well to metal bipyridine-based complexes.[34c] However, the luminescence lifetimes of the helicene complexes remain quite long, of the order of a few hundred nanoseconds (**Table 2**), suggesting that the low quantum yields might be due in part to reduction in the radiative rate rather than to particularly severe non-radiative decay. Indeed, estimation of the radiative and non-radiative rate constants, k_r and Σk_{nr}, indicates that the former is around an order of magnitude lower than for $[Ru(bipy)_3]^{2+}$. Such an effect could be attributed to reduced metal character in the excited state with increasingly conjugated ligands,[35a] and/or to changes in the relative energies of higher singlet and triplet states that couple through spin-orbit coupling.[35b] The emission is modestly quenched by dissolved molecular O_2 (as expected for lifetimes of this order of magnitude), with bimolecular rate constants of around 10^9 M^{-1} s^{-1}.

Although there is little difference between the spectra of the different diastereoisomers, it is intriguing to note a small but significant difference between the quantum yields and lifetimes of the diastereoisomers of **12**. The emission of the (*P*,Λ,Λ) isomer is brighter and longer-lived than that of the (*M*,Λ,Λ), apparently due largely to an almost 4-fold difference in Σk_{nr}. The difference most likely arises from the different conformation of the two complex units relative to one another, influencing exposure to solvent and hence excited-state deactivation pathways.[36]

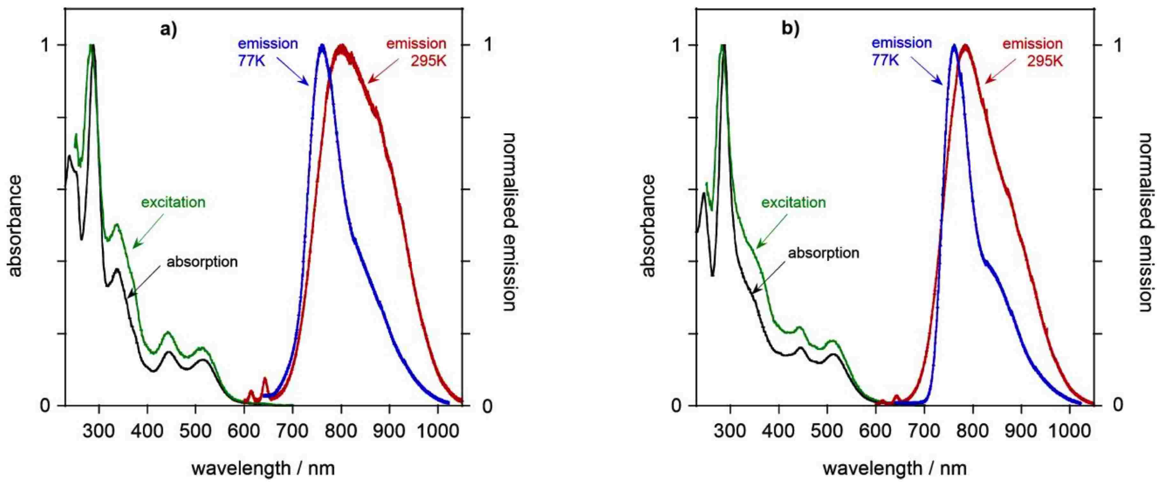

Figure 8. Absorption spectra (black), emission spectra (red), and excitation spectra (green) in MeCN at 295 K, and emission in PrCN at 77 K (blue), of a) (*M*,Δ)-**11c** and b) (*P*,Λ,Λ)-**12**. Corresponding spectra of other complexes are shown in SI (**Figures S54-S56**).

Table 2. Luminescence properties of the ruthenium(II) complexes[(a)]

Complex	Absorption λ_{max} / nm (ε / M^{-1} cm^{-1})	Emission λ_{max} / nm	Φ_{lum} / 10^{-2}	τ / ns (b)	k_r / 10^3 s^{-1} (c)	Σk_r / 10^6 s^{-1} (c)	k_Q^{O2} / 10^8 M^{-1} s^{-1} (d)	Emission at 77 K	
								λ_{max} / nm	τ / ns
(*rac*)-**11a**	289 (66700), 337 (19250), 405 (10800), 437 (13400), 510 (11400)	788	0.03	46 [40]	6.5	22	17	742	1800
(*P*,Δ)-**11c**	239 (44600), 289 (65300), 339 (23600), 446 (7835), 510 (6590)	779	0.10	290 [180]	3.4	3.4	11	728	1300
(*M*,Δ)-**11c**	239 (49830), 289 (60930), 337 (26580), 444 (9020), 515 (7470)	799	0.09	260 [180]	3.5	3.8	9.0	761	1400
(*M*,Λ,Λ)-**12**	246 (77300), 288 (139810), 435sh (21820), 522 (16810)	788	0.10	130 [110]	7.7	7.7	7.4	758, 840sh	1000
(*P*,Λ,Λ)-**12**	246 (65500), 287 (115850), 344sh (33200), 444 (18420), 512 (14230)	786	0.25	510 [340]	4.9	2.0	5.2	761, 837sh	1800

(a) In deoxygenated acetonitrile at 295 ± 1 K and in butyronitrile at 77 K. (b) Values in parenthesis are for air-equilibrated solution. (c) Values estimated assuming that the emitting triplet state is formed with unit efficiency upon excitation into the singlet bands, such that $k_r = \Phi / \tau$ and $\Sigma k_{nr} = (1-\Phi) / \tau$. (d) Bimolecular rate constants for quenching by O_2, estimated based on the lifetimes in deoxygenated and air-equilibrated solution.

UV-vis and ECD spectra of complexes 11a, 11c, and 12

The ECD spectra of the enantioenriched forms of **11a** in MeCN are mirror images of one another (**Figure 5b**). Enantiomer (Λ)-**11a** shows a positive band at 292 nm ($\Delta\varepsilon = +60$ M^{-1} cm^{-1}), a weak positive one at 245 nm ($\Delta\varepsilon = +24$ M^{-1} cm^{-1}), and two weak negative bands at 275 nm ($\Delta\varepsilon = -23$ M^{-1} cm^{-1}) and at 219 nm ($\Delta\varepsilon = -33$ M^{-1} cm^{-1}). Additionally, two negative ECD-bands of very low intensities ($\Delta\varepsilon = -2$ M^{-1} cm^{-1}) are found at 375 and 510 nm, i.e. in the MLCT region. The absolute stereochemistry can be easily deduced from starting enantioenriched Ru precursors and confirmed by comparison of ECD fingerprints at 292 nm with known chiral complexes.[30]

The ECD spectra of diastereo- and enantioenriched **11c** in MeCN are depicted and compared in **Figure 6b**. Both enantiomeric pairs (*P*,Λ)/(*M*,Δ)- and (*P*,Δ)/(*M*,Λ)-**11c** display mirror-image spectra.

(*P*,Λ)-**11c** exhibits more intense ECD signals with strong positive band at 291 nm (Δε = +120 M^{-1} cm^{-1}) accompanied by weaker positive band at 335 nm (Δε = +45 M^{-1} cm^{-1}), a strong negative band at 251 nm (Δε = −135 M^{-1} cm^{-1}), and weak bands at 523 nm (Δε = +8 M^{-1} cm^{-1}), 451 nm (Δε = −11 M^{-1} cm^{-1}), and 394 nm (Δε = +8 M^{-1} cm^{-1}). (*P*,Δ)-**11c** exhibits two strong positive bands at 344 nm (Δε = +60 M^{-1} cm^{-1}) and 275 nm (Δε = +70 M^{-1} cm^{-1}), two strong negative bands at 294 nm (Δε = −70 M^{-1} cm^{-1}) and 236 nm (Δε = −100 M^{-1} cm^{-1}), and weak bands at 507 nm (Δε = +17 M^{-1} cm^{-1}), 443 nm (Δε = −6 M^{-1} cm^{-1}), and 314 nm (Δε = +22 M^{-1} cm^{-1}). Overall, thanks to the presence of the hexahelix, the enantioenriched **11c** derivatives display more intense ECD responses than the **11a** ones.

The ECD spectra of diastereo- and enantioenriched **12** in MeCN are depicted and compared in **Figure 6d**. Both enantiomeric pairs (*P*,Λ,Λ)/(*M*,Δ,Δ)- and (*P*,Δ,Δ)/(*M*,Λ,Λ)-**12** display mirror-image spectra. Overall, the (*P*,Λ,Λ)- diastereomer shows less intense ECD signals with more crossing points than the (*P*,Δ,Δ)- one. (*P*,Λ,Λ)-**12** exhibits three strong bands at 277 nm (Δε = −150 M^{-1} cm^{-1}), 291 nm (Δε = +105 M^{-1} cm^{-1}) and 337 nm (Δε = +110 M^{-1} cm^{-1}), accompanied by several weak bands at 306 nm (Δε = −23 M^{-1} cm^{-1}), 435 nm (Δε = −24 M^{-1} cm^{-1}), 507 nm (Δε = +16 M^{-1} cm^{-1}), and 547 nm (Δε = −12 M^{-1} cm^{-1}). (*P*,Δ,Δ)-**12** displays one strong negative band at 294 nm (Δε = −295 M^{-1} cm^{-1}), one moderate positive band at 367 nm (Δε = +115 M^{-1} cm^{-1}), three weaker bands at 532 nm (Δε = +65 M^{-1} cm^{-1}), 277 nm (Δε = +55 M^{-1} cm^{-1}), and 266 (Δε = −50 M^{-1} cm^{-1}), and one weak band at 446 nm (Δε = −10 M^{-1} cm^{-1}). The heptahelicenic structure thus leads to a strong chiroptical response which is further increased through a synergistic contribution of the two Ru centers. It is worth to note that mirror-imaged ECD spectra were systematically obtained for each enantiomeric pair of **11a**, **11c** and **12**, which confirms that the reactions proceeded without loss of enantiopurity.

Spectroelectrochemical properties of complexes 11a, 11c, and 12

The electrochemical properties of complexes **11a**, **11c**, (*M*,Δ,Δ)- and (*M*,Λ,Λ)-**12** were studied by cyclic voltammetry recorded in MeCN under an inert atmosphere with 0.1 M Bu_4NPF_6 as the supporting electrolyte. The half-wave redox potentials were determined from the average of the anodic and cathodic peak potentials for the reversible waves. The cyclic voltammograms depicted in **Figure 9** reveal one reversible Ru(II)/Ru(III) oxidation wave at +1.14, +1.23 vs. SCE for complexes **11a** and **11c**, respectively. These values are very similar to those found in the literature for $[Ru(bipy)_3]^{2+}$,[19a,37a] while for the bis-Ru complex diastereomers (*M*,Δ,Δ)- and (*M*,Λ,Λ)-**12**, higher values were obtained (+1.31 and +1.26 V). Mono-ruthenium complexes **11a** and **11c** also display three reversible waves in reduction (−1.10, −1.60, and −1.86 V for **11a**; −1.05, −1.51, and −1.75 V for **11c**). These reduction potentials correspond to Ru(II)/Ru(I), Ru(I)/Ru(0), and Ru(0)/Ru(-1) one electron-reduction steps, and are found to be similar to the reduction potentials of $[Ru(bipy)_3]^{2+}$ systems.[19,23] The bis-ruthenium complexes (*M*,Δ,Δ)- and (*M*,Λ,Λ)-**12** appear easier to reduce and exhibit the first set of two reversible waves (−1.11 and −1.08 V) corresponding to the two Ru(II)/Ru(I) processes of the Ru atoms that do not reduce at the same potential, thus evidencing an electronic interaction between the two metal centers via the π-helicene bridge.[37b] Another two-electron reduction wave corresponding to the Ru(I)/Ru(0) reduction of the two Ru centers is also found (−1.50 to −1.48 V).

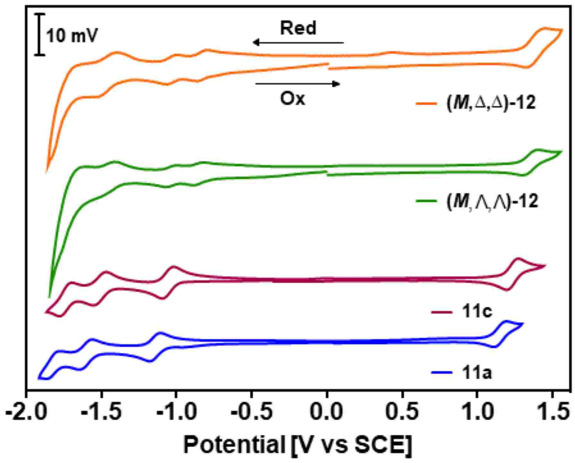

Figure 9. Cyclic voltammograms of **11a**, **11c**, (*M*,Δ,Δ)- and (*M*,Λ,Λ)-**12** in degassed MeCN (0.1 M Bu_4NPF_6) plotted versus the saturated calomel electrode (SCE), measured using ferrocene as an internal standard.

Redox-triggered chiroptical switching activity

Based on these results, it appeared interesting to take advantage of the reversible oxidation and reduction processes and to study the electrochromic and chiroptical switching activity of such complexes. For this purpose, enantioenriched complexes (Λ)-**11a**, (*P*,Δ)-**11c**, (*P*,Δ,Δ)- and (*P*,Λ,Λ)-**12** were examined. The one-electron oxidation process was first studied by UV-vis and ECD spectroscopies in an optically transparent thin-layer electrochemical (OTTLE) cell (MeCN/0.2 M Bu_4NPF_6) upon applying a potential up to c.a. 1.3 V (**Figure 10**, see the electrochemical conditions in SI). In all cases, several isosbestic points were observed in both UV-vis and ECD. Overall, the UV-vis spectra underwent a strong decrease of intensity of the high energy band around 290 nm. Oxidation was accompanied by a 15 nm red shift. In the higher energy domain, disappearance or decreasing of the broad absorption bands located between 440 and 520 nm was observed. In the ECD spectra, the strong positive band around 300 nm in (Λ)-**11a** and (*P*,Δ)-**11c** underwent a significant decrease accompanied by a c.a. 15 nm red shift, while the low-energy bands exhibited intensity decreases (see **Figures 10a** and **10b**). Diastereomeric complexes (*P*,Δ,Δ)- and (*P*,Λ,Λ)-**12** also evidenced similar changes (see **Figures 10c** and **10d**). In contrast to the UV-vis spectra, the effects in ECD were different for the two diastereomers. The oxidation of (*P*,Λ,Λ)-**12** resulted in an inversion of the positive band at 291 nm (Δε value moved from +105 to −70 M^{-1} cm^{-1}); the broad positive band at 337 nm was split into two less intense bands; and the two weak bands between 480 and 600 nm vanished. Upon oxidation of (*P*,Δ,Δ)-**12**, bands at 294 and 367 nm were red-shifted around 24 and 10 nm, respectively, and bands at 266, 277, and 532 nm disappeared.

Since the comparison between the ECD spectra of (*P*,Λ,Λ)-**12** in Ru(II) and Ru(III) oxidation state shows dramatic changes in the chiroptical properties, the possibility of using such a system as a chiroptical switch was explored. For (*P*,Λ,Λ)-**12**, the difference between Δε values at 290 nm is not only significant (□170 M^{-1} cm^{-1}) but also accompanied by a change in sign. Therefore, it may be considered as a +/− chiroptical switch. The reversibility of switching was further proved by several cycles of oxidation and reduction of (*P*,Λ,Λ)-**12** in MeCN, which were accompanied by a modulation of the ECD signal upon applying potential steps between 0.8 and 1.3 V (**Figure 11**). The helicene-bipy-Ru complexes described here thus constitute a new class of helicene-based redox-triggered chiroptical switches.[38] Due to the presence of several simultaneous redox steps, the multiple electrons reduction processes of (Λ)-**11a**, (*P*,Δ)-**11c**, an (*P*,Δ,Δ)- and (*P*,Λ,Λ)-**12**, resulted in less significant and less clear changes, as compared to the one-electron oxidation. The spectroelectrochemical reduction processes are thus more difficult to interpret (for selected spectra, see **Figures S57-58** in SI).

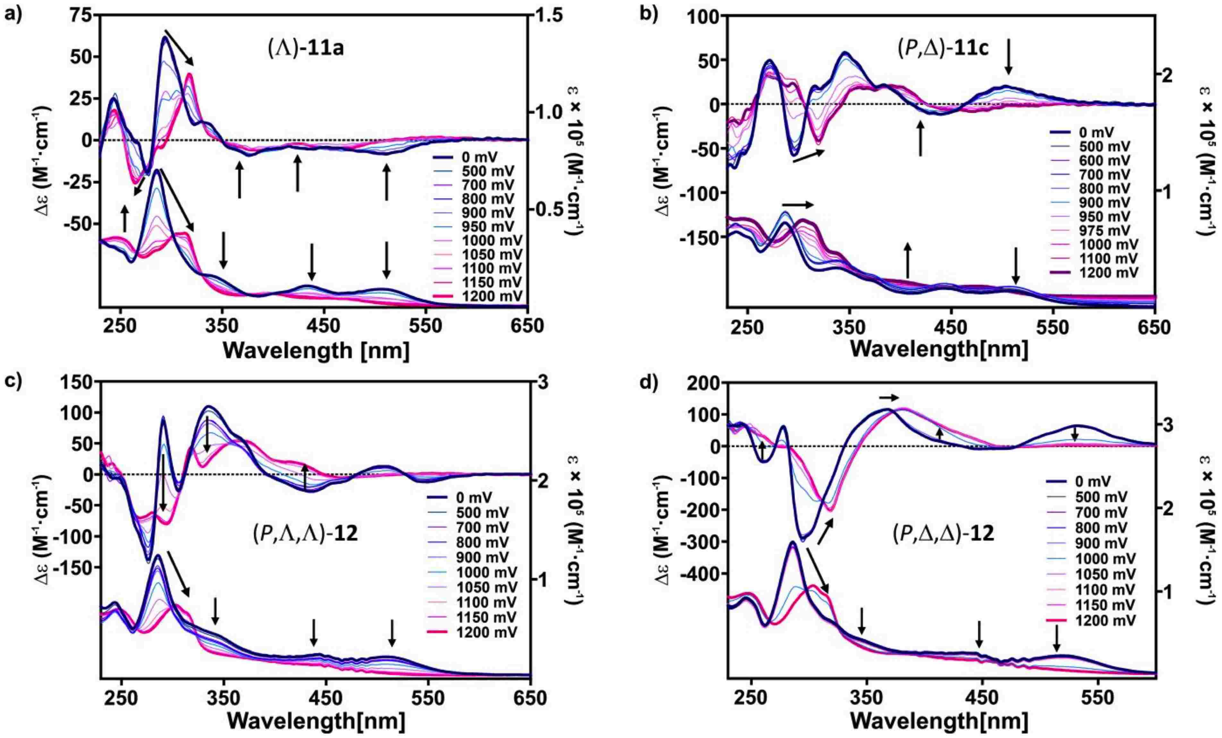

Figure 10. Spectroelectrochemical studies UV-vis (bottom) and ECD (up) studies of oxidation processes of a) (Λ)-**11a**, b) (*P*,Δ)-**11c**, c) (*P*,Λ,Λ)-**12** and d) (*P*,Δ,Δ)-**12** (OTTLE cell, MeCN, 0.2 M Bu_4NPF_6).

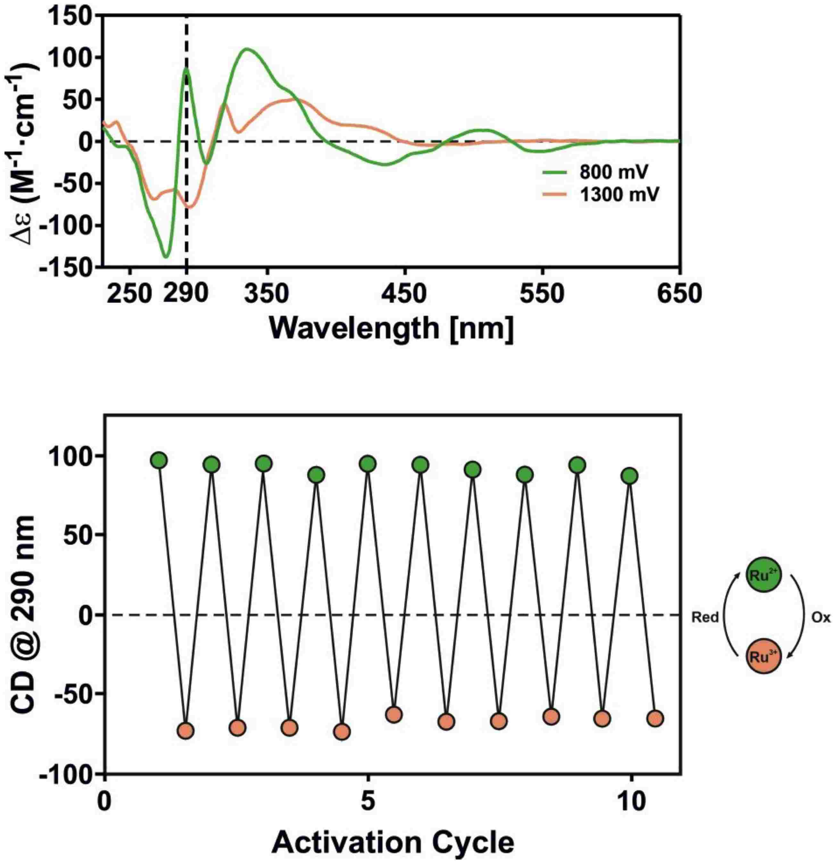

Figure 11. Redox-triggered chiroptical switching process of (*P*,Λ,Λ)-**12** following the ECD value at 290 nm (□10^{-3} M, Bu_4NPF_6).

Conclusions

In summary, we have shown that photocyclization of aromatic imines is a suitable method for the preparation of helicenes decorated with one or two bipy-moieties. Formation of aza[6]- and aza[7]helicenes displaying one or two complexing bipy units was accessed for the first time by this methodology. These ligands were used for the preparation of chiral ruthenium(II) complexes in diastereo- and enantioenriched forms, which were subsequently characterized. The coordination of bipy-helicenes to the ruthenium ion generates fused metallic bis- or tris-helicenic systems. The stereochemistry of these compounds has been examined in details through their X-ray crystallographic structures. Spectroelectrochemical UV-vis and ECD studies of the prepared complexes revealed their extensive redox-modulated chiroptical properties. Due to the strong reversible changes in the ECD spectra upon oxidation of the bis-ruthenium complex, the system may be considered as a redox-triggered chiroptical switch. The above-described complexes open up new possibilities in the search of other helicenes with switchable redox and optical properties and will be further studied in this regard.

Author Contributions

M.K. performed the synthesis of ligands and complexes, R.R. performed CD, CPL, and spectroelectochemical studies, J.V. performed HPLC separation of ligands, I.C., M.C., E.C., and J.Sy. performed structural analysis (X-ray and NMR), J.A.G.W. performed non-polarized luminescence studies, V.C., J.St., and J.Z. designed synthesis of helicenes and were involved in supervision and revision and editing of the manuscript, J.C. designed the synthesis of complexes and wrote/revised together with other authors the manuscript.

Conflicts of interest

There are no conflicts to declare.

Acknowledgments

We thank the Centre National de la Recherche Scientifique (CNRS) and the University of Rennes. This work was supported by the Czech Science Foundation (grant no. 20-19353S). M.K. is grateful to the Ministry of Education, Youth and Sports of the Czech Republic and EU—European Structural and Investment Funds—Operational Programme Research, Development, and Education for the project ÚCHP Mobilita II (CZ.02.2.69/0.0/0.0/18_053/0016920). R.R. thanks Xunta de Galicia for a Postdoctoral fellowship. The authors thank Sitthichok Kasemthaveechok from University of Rennes 1 for help with electrochemical measurements. NMR and ECD experiments were performed on the PRISM core Facility (Biogenouest, UMS Biosit, Université de Rennes 1).

Supporting Information

The available Supporting Information file includes General Information on material and methods used, synthetic procedures, chiral separations, and characterization data (NMR, X-ray, optical rotation values, spectroelectrochemical data, and additional spectral information).

References

1. a) Shen, Y.; Chen, C. F. Helicenes: Synthesis and Applications. *Chem. Rev.* **2012**, *112* (3), 1463–1535. https://doi.org/10.1021/cr200087r.
   b) Chen, C.-F.; Shen, Y. *Helicene Chemistry*; Springer Berlin Heidelberg, 2017. https://doi.org/10.1007/978-3-662-53168-6. c) Gingras, M. One Hundred Years of Helicene Chemistry. Part 1: Non-Stereoselective Syntheses of Carbohelicenes. *Chem. Soc. Rev.* **2013**, *42* (3), 968–1006. https://doi.org/10.1039/C2CS35154D.
2. Selected examples: a) Carreño, M. C.; Enríquez, Á.; García-Cerrada, S.; Sanz-Cuesta, M. J.; Urbano, A.; Maseras, F.; Nonell-Canals, A.; Towards Configurationally Stable [4]Helicenes: Enantioselective Synthesis of 12-Substituted 7,8-Dihydro[4]Helicene Quinones. *Chem. - A Eur. J.* **2008**, *14* (2), 603–620. https://doi.org/10.1002/chem.200700762.; b) Delgado, I. H.; Pascal, S.; Wallabregue, A.; Duwald, R.; Besnard, C.; Guénée, L.; Nançoz, C.; Vauthey, E.; Tovar, R. C.; Lunkley, J. L.; Muller, G.; Lacour, J. Functionalized Cationic [4]Helicenes with Unique Tuning of Absorption, Fluorescence and Chiroptical Properties up to the Far-Red Range. *Chem. Sci.* **2016**, *7* (7), 4685–4693. https://doi.org/10.1039/C6SC00614K.; c) Hartung, T.; Machleid, R.; Simon, M.; Golz, C.; Alcarazo, M.; Enantioselective Synthesis of 1,12-Disubstituted [4]Helicenes. *Angew. Chemie Int. Ed.*, **2020**, *59* (14), 5660–5664. https://doi.org/10.1002/anie.201915870.
3. a) Gingras, M. One Hundred Years of Helicene Chemistry. Part 3: Applications and Properties of Carbohelicenes. *Chem. Soc. Rev.* **2013**, *42* (3), 1051–1095. https://doi.org/10.1039/C2CS35134J.

; b) Dhbaibi, K.; Favereau, L.; Crassous, J. Enantioenriched Helicenes and Helicenoids Containing Main-Group Elements (B, Si, N, P). *Chem. Rev.* **2019**, *119* (14), 8846–8953. https://doi.org/10.1021/acs.chemrev.9b00033.

4. a) Yang, Y.; da Costa, R. C.; Smilgies, D.-M.; Campbell, A. J.; Fuchter, M. J.; Induction of Circularly Polarized Electroluminescence from an Achiral Light-Emitting Polymer via a Chiral Small-Molecule Dopant. Adv. Mater. **2013**, *25* (18), 2624–2628. https://doi.org/10.1002/adma.201204961.; b) Zhao, W.-L.; Li, M.; Lu, H.-Y.; Chen, C.-F. Advances in Helicene Derivatives with Circularly Polarized Luminescence. *Chem. Commun.* **2019**, *55* (92), 13793–13803. https://doi.org/10.1039/C9CC06861A.; c) J. Crassous, in *Circularly Polarized Luminescence of Isolated Small Organic Molecules*, ed. T. Mori, Springer Singapore, Singapore, 2020, pp. 53–97.
5. Yang, Y.; Da Costa, R. C.; Smilgies, D. M.; Campbell, A. J.; Fuchter, M. J. Induction of Circularly Polarized Electroluminescence from an Achiral Light-Emitting Polymer via a Chiral Small-Molecule Dopant. *Adv. Mater.* **2013**, *25* (18), 2624–2628. https://doi.org/10.1002/adma.201204961.
6. Kiran, V.; Mathew, S. P.; Cohen, S. R.; Hernández Delgado, I.; Lacour, J.; Naaman, R. Helicenes-A New Class of Organic Spin Filter. *Adv. Mater.* **2016**, *28* (10), 1957–1962. https://doi.org/10.1002/adma.201504725.
7. a) Saleh, N.; Shen, C.; Crassous, J. Helicene-Based Transition Metal Complexes: Synthesis, Properties and Applications. *Chem. Sci.* **2014**, *5* (10), 3680–3694. https://doi.org/10.1039/C4SC01404A.; b) OuYang, J.; Crassous, J. Chiral Multifunctional Molecules Based on Organometallic Helicenes: Recent Advances. *Coord. Chem. Rev.* **2018**, *376*, 533–547. https://doi.org/10.1016/j.ccr.2018.08.015.; c) Gauthier, E. S.; Rodríguez, R.; Crassous, J. Metal-Based Multihelicenic Architectures. *Angew. Chemie Int. Ed.* **2020**, *59* (51), 22840–22856. https://doi.org/10.1002/anie.202004361.
8. Saleh, N.; Moore, B.; Srebro, M.; Vanthuyne, N.; Toupet, L.; Williams, J. A. G.; Roussel, C.; Deol, K. K.; Muller, G.; Autschbach, J.; Crassous, J. Acid/Base-Triggered Switching of Circularly Polarized Luminescence and Electronic Circular Dichroism in Organic and Organometallic Helicenes. *Chem. - Eur. J.* **2015**, *21* (4), 1673–1681. https://doi.org/10.1002/chem.201405176.
9. a) Norel, L.; Rudolph, M.; Vanthuyne, N.; Williams, J. A. G.; Lescop, C.; Roussel, C.; Autschbach, J.; Crassous, J.; Réau, R. Metallahelicenes: Easily Accessible Helicene Derivatives with Large and Tunable Chiroptical Properties. *Angew. Chem. Int. Ed.* **2010**, *49* (1), 99–102. https://doi.org/10.1002/anie.200905099.; b) Shen, C.; Anger, E.; Srebro, M.; Vanthuyne, N.; Deol, K. K.; Jefferson, T. D.; Muller, G.; Williams, J. A. G.; Toupet, L.; Roussel, C.; Autschbach, J.; Réau, R.; Crassous, J. Straightforward Access to Mono- and Bis-Cycloplatinated Helicenes Displaying Circularly Polarized Phosphorescence by Using Crystallization Resolution Methods. *Chem. Sci.* **2014**, *5* (5), 1915–1927. https://doi.org/10.1039/c3sc53442a.; c) Brandt, J. R.; Wang, X.; Yang, Y.; Campbell, A. J.; Fuchter, M. J. Circularly Polarized Phosphorescent Electroluminescence with a High Dissymmetry Factor from PHOLEDs Based on a Platinahelicene. *J. Am. Chem. Soc.* **2016**, *138* (31), 9743–9746. https://doi.org/10.1021/jacs.6b02463.
10. Kaes, C.; Katz, A.; Hosseini, M. W. Bipyridine: The Most Widely Used Ligand. A Review of Molecules Comprising at Least Two 2,2‘-Bipyridine Units. *Chem. Rev.* **2000**, *100* (10), 3553–3590. https://doi.org/10.1021/cr990376z.
11. Chen, J.; Captain, B.; Takenaka, N. Helical Chiral 2,2′-Bipyridine *N*-Monoxides as Catalysts in the Enantioselective Propargylation of Aldehydes with Allenyltrichlorosilane. *Org. Lett.* **2011**, *13* (7), 1654–1657. https://doi.org/10.1021/ol200102c.

12. Klívar, J.; Šámal, M.; Jančařík, A.; Vacek, J.; Bednárová, L.; Buděšínský, M.; Fiedler, P.; Starý, I.; Stará, I. G. Asymmetric Synthesis of Diastereo- and Enantiopure Bioxahelicene 2,2′-Bipyridines. *Eur. J. Org. Chem.* **2018**, *2018* (37), 5164–5178. https://doi.org/10.1002/ejoc.201800541.
13. Kaneko, E.; Matsumoto, Y.; Kamikawa, K. Synthesis of Azahelicene *N*-Oxide by Palladium-Catalyzed Direct C-H Annulation of a Pendant (*Z*)-Bromovinyl Side Chain. *Chem. - Eur. J.* **2013**, *19* (36), 11837–11841. https://doi.org/10.1002/chem.201302083.
14. Isla, H.; Saleh, N.; Ou-Yang, J. K.; Dhbaibi, K.; Jean, M.; Dziurka, M.; Favereau, L.; Vanthuyne, N.; Toupet, L.; Jamoussi, B.; Srebro-Hooper, M.; Crassous, J. Bis-4-Aza[6]Helicene: A Bis-Helicenic 2,2′-Bipyridine with Chemically Triggered Chiroptical Switching Activity. *J. Org. Chem.* **2019**, *84* (9), 5383–5393. https://doi.org/10.1021/acs.joc.9b00389.
15. a) Saleh, N.; Srebro, M.; Reynaldo, T.; Vanthuyne, N.; Toupet, L.; Chang, V. Y.; Muller, G.; Williams, J. A. G.; Roussel, C.; Autschbach, J.; Crassous, J. Enantio-Enriched CPL-Active Helicene–Bipyridine–Rhenium Complexes. *Chem. Commun.* **2015**, *51* (18), 3754–3757. https://doi.org/10.1039/C5CC00453E.; b) Saleh, N.; Kundu, D.; Vanthuyne, N.; Olesiak-Banska, J.; Pniakowska, A.; Matczyszyn, K.; Chang, V. Y.; Muller, G.; Williams, J. A. G.; Srebro-Hooper, M.; Autschbach, J.; Crassous, J. Dinuclear Rhenium Complexes with a Bridging Helicene-bis-bipyridine Ligand: Synthesis, Structure, and Photophysical and Chiroptical Properties. *Chempluschem* **2020**, *85* (11), 2446–2454. https://doi.org/10.1002/cplu.202000559.
16. Saleh, N.; Srebro, M.; Reynaldo, T.; Vanthuyne, N.; Toupet, L.; Chang, V. Y.; Muller, G.; Williams, J. A. G.; Roussel, C.; Autschbach, J.; Crassous, J. Enantio-Enriched CPL-Active Helicene–Bipyridine–Rhenium Complexes. *Chem. Commun.* **2015**, *51* (18), 3754–3757. https://doi.org/10.1039/C5CC00453E.
17. a) Ou-Yang, J.-K.; Saleh, N.; Fernandez Garcia, G.; Norel, L.; Pointillart, F.; Guizouarn, T.; Cador, O.; Totti, F.; Ouahab, L.; Crassous, J.; Le Guennic, B. Improved Slow Magnetic Relaxation in Optically Pure Helicene-Based Dy III Single Molecule Magnets. *Chem. Commun.* **2016**, *52* (100), 14474–14477. https://doi.org/10.1039/C6CC08638A.; b) Fernandez-Garcia, G.; Flores Gonzalez, J.; Ou-Yang, J.-K.; Saleh, N.; Pointillart, F.; Cador, O.; Guizouarn, T.; Totti, F.; Ouahab, L.; Crassous, J.; Le Guennic, B. Slow Magnetic Relaxation in Chiral Helicene-Based Coordination Complex of Dysprosium. *Magnetochemistry* **2016**, *3* (1), 2. https://doi.org/10.3390/magnetochemistry3010002.; c) Flores Gonzalez, J.; Montigaud, V.; Saleh, N.; Cador, O.; Crassous, J.; le Guennic, B.; Pointillart, F. Slow Relaxation of the Magnetization in Bis-Decorated Chiral Helicene-Based Coordination Complexes of Lanthanides. *Magnetochemistry* **2018**, *4* (3), 39. https://doi.org/10.3390/magnetochemistry4030039.; d) Galland, M.; Riobé, F.; Ouyang, J.; Saleh, N.; Pointillart, F.; Dorcet, V.; Le Guennic, B.; Cador, O.; Crassous, J.; Andraud, C.; Monnereau, C.; Maury, O. Helicenic Complexes of Lanthanides: Influence of the f-Element on the Intersystem Crossing Efficiency and Competition between Luminescence and Oxygen Sensitization. *Eur. J. Inorg. Chem.* **2019**, *2019* (1), 118–125. https://doi.org/10.1002/ejic.201800922.; e) Atzori, M.; Dhbaibi, K.; Douib, H.; Grasser, M.; Dorcet, V.; Breslavetz, I.; Paillot, K.; Cador, O.; Rikken, G. L. J. A.; Le Guennic, B.; Crassous, J.; Pointillart, F.; Train, C. Helicene-Based Ligands Enable Strong Magneto-Chiral Dichroism in a Chiral Ytterbium Complex. *J. Am. Chem. Soc.* **2021**, *143* (7), 2671–2675. https://doi.org/10.1021/jacs.0c13180.
18. a) Juris, A.; Balzani, V.; Barigelletti, F.; Campagna, S.; Belser, P.; von Zelewsky, A. Ru(II) Polypyridine Complexes: Photophysics, Photochemistry, Eletrochemistry, and Chemiluminescence. *Coord. Chem. Rev.* **1988**, *84* (C), 85–277. https://doi.org/10.1016/0010-8545(88)80032-8.; b) Balzani, V.; Credi, A.; Scandola, F. *Transition Metals in Supramolecular Chemistry*; Fabbrizzi, L., Poggi, A., Eds.; Springer Netherlands: Dordrecht, 1994. https://doi.org/10.1007/978-94-015-8380-0.; c) Balzani, V.; Juris, A.; Venturi, M.; Campagna, S.;

Serroni, S. Luminescent and Redox-Active Polynuclear Transition Metal Complexes. *Chem. Rev.* **1996**, *96* (2), 759–834. https://doi.org/10.1021/cr941154y.

19. Selected examples. Photochemistry: a) Sato, H.; Yamagishi, A. Application of the ΔΛ Isomerism of Octahedral Metal Complexes as a Chiral Source in Photochemistry. *J. Photochem. Photobiol. C Photochem. Rev.* **2007**, *8* (2), 67–84. https://doi.org/10.1016/j.jphotochemrev.2007.04.001.; Photocatalysis: b) Ohkubo, K.; Hamada, T.; Ishida, H. Novel Enantioselective Photocatalysis by Chiral, Helical Ruthenium(II) Complexes. *J. Chem. Soc. Chem. Commun.* **1993**, *3* (18), 1423.; c) Teplý, F. Photoredox Catalysis by [Ru(bpy)$_3$]$^{2+}$ to Trigger Transformations of Organic Molecules. Organic Synthesis Using Visible-Light Photocatalysis and Its 20th Century Roots. *Collect. Czechoslov. Chem. Commun.* **2011**, *76* (7), 859–917. https://doi.org/10.1135/cccc2011078.; Electrochromism: d) Puodziukynaite, E.; Oberst, J. L.; Dyer, A. L.; Reynolds, J. R. Establishing Dual Electrogenerated Chemiluminescence and Multicolor Electrochromism in Functional Ionic Transition-Metal Complexes. *J. Am. Chem. Soc.* **2012**, *134* (2), 968–978. https://doi.org/10.1021/ja2065297. Electrochemiluminescence: e) Voci, S.; Zinna, F.; Arrico, L.; Grass, S.; Bouffier, L.; Lacour, J.; Di Bari, L.; Sojic, N. Chiroptical Detection of a Model Ruthenium Dye in Water by Circularly Polarized-Electrochemiluminescence. *Chem. Commun.* **2020**, *56* (44), 5989–5992. https://doi.org/10.1039/D0CC01571G. DNA binding: f) Mei, W. J.; Liu, J.; Zheng, K. C.; Lin, L. J.; Chao, H.; Li, A. X.; Yun, F. C.; Ji, L. N. Experimental and Theoretical Study on DNA-Binding and Photocleavage Properties of Chiral Complexes Δ- and Λ-[Ru(Bpy)$_2$L] (L = *o*-hpip, *m*-hpip and *p*-hpip) *Dalton Trans.* **2003**, No. 7, 1352–1359. https://doi.org/10.1039/b212443b.; g) Shi, S.; Xu, J.-H.; Gao, X.; Huang, H.-L.; Yao, T.-M. Binding Behaviors for Different Types of DNA G-Quadruplexes: Enantiomers of [Ru(Bpy)$_2$(L)]$^{2+}$ (L=dppz, Dppz-Idzo). *Chem. - Eur. J.* **2015**, *21* (32), 11435–11445. https://doi.org/10.1002/chem.201501093.
20. a) Chelucci, G.; Thummel, R. P. Chiral 2,2‘-Bipyridines, 1,10-Phenanthrolines, and 2,2‘:6‘,2‘ ‘-Terpyridines: Syntheses and Applications in Asymmetric Homogeneous Catalysis. *Chem. Rev.* **2002**, *102* (9), 3129–3170. https://doi.org/10.1021/cr0101914.; b) Fletcher, N. C. Chiral 2,2′-Bipyridines: Ligands for Asymmetric Induction. *J. Chem. Soc., Perkin Trans. 1* **2002**, *2* (16), 1831–1842. https://doi.org/10.1039/B204272J.; c) von Zelewsky, A. *Stereochemistry of Coordination Compounds*, J. & Wiley & Sons, Chichester, 1996; d) Amouri, H.; Gruselle, M. *Chirality in Transition Metal Chemistry*; John Wiley & Sons, Ltd: Chichester, UK, 2008. https://doi.org/10.1002/9780470721599.
21. Kos, M.; Žádný, J.; Storch, J.; Církva, V.; Cuřínová, P.; Sýkora, J.; Císařová, I.; Kuriakose, F.; Alabugin, I. V. Oxidative Photocyclization of Aromatic Schiff Bases in Synthesis of Phenanthridines and Other Aza-PAHs. *Int. J. Mol. Sci.* **2020**, *21* (16), 5868. https://doi.org/10.3390/ijms21165868.
22. a) Badger, G. M.; Joshua, C. P.; Lewis, G. E. Photocatalysed Cyclization of Benzalaniline. *Tetrahedron Lett.* **1964**, *5* (49), 3711–3713. https://doi.org/10.1016/S0040-4039(01)89365-5.; b) Thompson, C. M.; Docter, S. Lewis Acid Promoted Photocyclization of Arylimines. Studies Directed towards the Synthesis of Pentacyclic Natural Products. *Tetrahedron Lett.* **1988**, *29* (41), 5213–5216. https://doi.org/10.1016/S0040-4039(00)80719-4.
23. a) Howarth, J.; Finnegan, J. The Synthesis of 9, 10-Dimethyl[7]Helicene and 8, 11-Diaza[7]Helicene. *Synth. Commun.* **1997**, *27* (20), 3663–3668. https://doi.org/10.1080/00397919708007089.; b) Caronna, T.; Gabbiadini, S.; Mele, A.; Recupero, F. Approaches to the Azahelicene System: Synthesis and Spectroscopic Characterization of Some Diazapentahelicenes. *Helv. Chim. Acta* **2002**, *85* (1), 1–8. https://doi.org/10.1002/1522-2675(200201)85:1<1::AID-HLCA1>3.0.CO;2-C.
24. Ghosh, A.; Csókás, D.; Budanović, M.; Webster, R. D.; Pápai, I.; Stuparu, M. C. Synthesis of Azahelicenes through Mallory Reaction of Imine Precursors: Corannulene Substrates Provide an

Exception to the Rule in Oxidative Photocyclizations of Diarylethenes. *Chem. Sci.* **2021**. https://doi.org/10.1039/D0SC06730J.

25. a) Li, C.; Yang, Y.; Miao, Q. Recent Progress in Chemistry of Multiple Helicenes. *Chem. - Asian J.* **2018**, *13* (8), 884–894. https://doi.org/10.1002/asia.201800073.; b) Kato, K.; Segawa, Y.; Itami, K. Symmetric Multiple Carbohelicenes. *Synlett* **2019**, *30* (04), 370–377. https://doi.org/10.1055/s-0037-1610283.; c) Mori, T. Chiroptical Properties of Symmetric Double, Triple, and Multiple Helicenes. *Chem. Rev.* **2021**, *121* (4), 2373–2412. https://doi.org/10.1021/acs.chemrev.0c01017.
26. a) Cortijo, M.; Viala, C.; Reynaldo, T.; Favereau, L.; Fabing, I.; Srebro-Hooper, M.; Autschbach, J.; Ratel-Ramond, N.; Crassous, J.; Bonvoisin, J. Synthesis, Spectroelectrochemical Behavior, and Chiroptical Switching of Tris(β-Diketonato) Complexes of Ruthenium(III), Chromium(III), and Cobalt(III). *Inorg. Chem.* **2017**, *56* (8), 4555–4567. https://doi.org/10.1021/acs.inorgchem.6b03094.; b) Li, D.; Wang, Z. Y.; Ma, D. Electrically-Controlled near-Infrared Chiroptical Switching of Enantiomeric Dinuclear Ruthenium Complexes. *Chem. Commun.* **2009**, No. 12, 1529. https://doi.org/10.1039/b819270g.; c) Feringa, B. L.; Browne, W. R. *Molecular Switches*, Wiley-VCH Verlag GmbH & Co. KGaA, Weinheim, Germany, 2011, vol. 1. https://doi.org/10.1002/9783527634408.; d) Canary, J. W. Redox-Triggered Chiroptical Molecular Switches. *Chem. Soc. Rev.* **2009**, *38* (3), 747. https://doi.org/10.1039/b800412a.
27. Hoffmann, N. Photochemical Reactions Applied to the Synthesis of Helicenes and Helicene-like Compounds. *J. Photochem. Photobiol. C Photochem. Rev.* **2014**, *19* (1), 1–19. https://doi.org/10.1016/j.jphotochemrev.2013.11.001.
28. R Martin, R. H.; Marchant, M. J. Thermal Racemisation of Hepta-, Octa-, and Nonahelicene. *Tetrahedron* **1974**, *30* (2), 347–349. https://doi.org/10.1016/S0040-4020(01)91469-3.
29. a) Ghosh, P.; Spiro, T. G. Photoelectrochemistry of Tris(Bipyridyl)Ruthenium(II) Covalently Attached to n-Type Tin(IV) Oxide. *J. Am. Chem. Soc.* **1980**, *102* (17), 5543–5549. https://doi.org/10.1021/ja00537a021.; b) Martínez, M. Á.; Carranza, M. P.; Massaguer, A.; Santos, L.; Organero, J. A.; Aliende, C.; de Llorens, R.; Ng-Choi, I.; Feliu, L.; Planas, M.; Rodríguez, A. M.; Manzano, B. R.; Espino, G.; Jalón, F. A. Synthesis and Biological Evaluation of Ru(II) and Pt(II) Complexes Bearing Carboxyl Groups as Potential Anticancer Targeted Drugs. *Inorg. Chem.* **2017**, *56* (22), 13679–13696. https://doi.org/10.1021/acs.inorgchem.7b01178.
30. Tartrate resolving agent: a) Hua, X.; von Zelewsky, A. Enantiomerically Pure Chiral $\mathrm{Ru^{II}(L\text{-}L)_2}$ Building Blocks for Coordination Compounds. *Inorg. Chem.* **1995**, *34* (23), 5791–5797. https://doi.org/10.1021/ic00127a017.; b) Hua, X.; Von Zelewsky, A. First Stereospecific Preparation of a Polynuclear Coordination Compound. Use of Λ-Bis(o-Phenanthroline)Ruthenium(II) as a Chiral Building Block. *Inorg. Chem.* **1991**, *30* (20), 3796–3798. https://doi.org/10.1021/ic00020a005. TRISPHAT resolving agent: c) Lacour, J.; Torche-Haldimann, S.; Jodry, J. J. Ion Pair Chromatographic Resolution of Tris(Diimine)Ruthenium(II) Complexes Using TRISPHAT Anions as Resolving Agents. *Chem. Commun.* **1998**, No. 16, 1733–1734. https://doi.org/10.1039/a803904f.; Chiral Sulfoxide resolving agent: d) Hesek, D.; Inoue, Y.; Ishida, H.; Everitt, S. R. .; Drew, M. G. . The First Asymmetric Synthesis of Chiral Ruthenium Tris(Bipyridine) from Racemic Ruthenium Bis(Bipyridine) Complexes. *Tetrahedron Lett.* **2000**, *41* (15), 2617–2620. https://doi.org/10.1016/S0040-4039(00)00230-6.
31. a) Evans, D. H.; O'Connell, K. M.; Petersen, R. A.; Kelly, M. J. Cyclic Voltammetry. *J. Chem. Educ.* **1983**, *60* (4), 290. https://doi.org/10.1021/ed060p290; b) (1) Damrauer, N. H. Femtosecond Dynamics of Excited-State Evolution in $[\mathrm{Ru(Bpy)_3}]^{2+}$. *Science* **1997**, *275* (5296), 54–57. https://doi.org/10.1126/science.275.5296.54.

32. Campagna, S.; Puntoriero, F.; Nastasi, F.; Bergami, G.; Balzani, V. Photochemistry and Photophysics of Coordination Compounds: Ruthenium, *Top. Curr. Chem.,* 2007, **280**, 117–214. https://doi.org/10.1007/128_2007_133
33. Barigelletti, F.; Juris, A.; Balzani, V.; Belser, P.; Von Zelewsky, A. Influence of the Ligand Structure on the Electrochemical and Spectroscopic Properties of Ruthenium(II)-Polypyridine Complexes. *Inorg. Chem.* **1987**, *26* (24), 4115–4119. https://doi.org/10.1021/ic00271a029.
34. a) Schulze, M.; Steffen, A.; Würthner, F. Near-IR Phosphorescent Ruthenium(II) and Iridium(III) Perylene Bisimide Metal Complexes. *Angew. Chemie Int. Ed.* **2015**, *54* (5), 1570–1573. https://doi.org/10.1002/anie.201410437.; b) Caspar, J. V.; Meyer, T. J. Photochemistry of Ru(Bpy)$_3^{2+}$. Solvent Effects. *J. Am. Chem. Soc.* **1983**, *105* (17), 5583–5590. https://doi.org/10.1021/ja00355a009.; c) Caspar, J. V.; Meyer, T. J. Application of the Energy Gap Law to Nonradiative, Excited-State Decay. *J. Phys. Chem.* **1983**, *87* (6), 952–957. https://doi.org/10.1021/j100229a010.
35. a) Kozhevnikov, D. N.; Kozhevnikov, V. N.; Shafikov, M. Z.; Prokhorov, A. M.; Bruce, D. W.; Williams, J. A. G. Phosphorescence vs Fluorescence in Cyclometalated Platinum(II) and Iridium(III) Complexes of (Oligo)Thienylpyridines. *Inorg. Chem.* **2011**, *50* (8), 3804–3815. https://doi.org/10.1021/ic200210e.; b) Escudero, D.; Happ, B.; Winter, A.; Hager, M. D.; Schubert, U. S.; González, L. The Radiative Decay Rates Tune the Emissive Properties of Ruthenium(II) Polypyridyl Complexes: A Computational Study. *Chem. - Asian J.* **2012**, *7* (4), 667–671. https://doi.org/10.1002/asia.201100864.
36. Gauthier, E. S.; Abella, L.; Hellou, N.; Darquié, B.; Caytan, E.; Roisnel, T.; Vanthuyne, N.; Favereau, L.; Srebro-Hooper, M.; Williams, J. A. G.; Autschbach, J.; Crassous, J. Long-Lived Circularly Polarized Phosphorescence in Helicene-NHC Rhenium(I) Complexes: The Influence of Helicene, Halogen, and Stereochemistry on Emission Properties. *Angew. Chem. Int. Ed.* **2020**, *59* (22), 8394–8400. https://doi.org/10.1002/anie.202002387.
37. a) Hohloch, S.; Schweinfurth, D.; Sommer, M. G.; Weisser, F.; Deibel, N.; Ehret, F.; Sarkar, B. The Redox Series [Ru(Bpy)$_2$(L)]$_n$, n = +3, +2, +1, 0, with L = Bipyridine, “Click” Derived Pyridyl-Triazole or Bis-Triazole: A Combined Structural, Electrochemical, Spectroelectrochemical and DFT Investigation. *Dalton Trans.* **2014**, *43* (11), 4437–4450. https://doi.org/10.1039/c3dt52898g.; b) Connelly, N. G.; Geiger, W. E. Chemical Redox Agents for Organometallic Chemistry. *Chem. Rev.* **1996**, *96* (2), 877–910. https://doi.org/10.1021/cr940053x.; c) Aguirre-Etcheverry, P.; O’Hare, D. Electronic Communication through Unsaturated Hydrocarbon Bridges in Homobimetallic Organometallic Complexes. *Chem. Rev.* **2010**, *110* (8), 4839–4864. https://doi.org/10.1021/cr9003852.; d) Costuas, K.; Rigaut, S. Polynuclear Carbon-Rich Organometallic Complexes: Clarification of the Role of the Bridging Ligand in the Redox Properties. *Dalt. Trans.* **2011**, *40* (21), 5643–5658. https://doi.org/10.1039/c0dt01388a.
38. a) Anger, E.; Srebro, M.; Vanthuyne, N.; Toupet, L.; Rigaut, S.; Roussel, C.; Autschbach, J.; Crassous, J.; Réau, R. Ruthenium-Vinylhelicenes: Remote Metal-Based Enhancement and Redox Switching of the Chiroptical Properties of a Helicene Core. *J. Am. Chem. Soc.* **2012**, *134* (38), 15628–15631. https://doi.org/10.1021/ja304424t.; b) Biet, T.; Fihey, A.; Cauchy, T.; Vanthuyne, N.; Roussel, C.; Crassous, J.; Avarvari, N. Ethylenedithio–Tetrathiafulvalene–Helicenes: Electroactive Helical Precursors with Switchable Chiroptical Properties. *Chem. - Eur. J.* **2013**, *19* (39), 13160–13167. https://doi.org/10.1002/chem.201301095.; c) Schweinfurth, D.; Zalibera, M.; Kathan, M.; Shen, C.; Mazzolini, M.; Trapp, N.; Crassous, J.; Gescheidt, G.; Diederich, F. Helicene Quinones: Redox-Triggered Chiroptical Switching and Chiral Recognition of the Semiquinone Radical Anion Lithium Salt by Electron Nuclear Double Resonance Spectroscopy. *J. Am. Chem. Soc.* **2014**, *136* (37), 13045–13052. https://doi.org/10.1021/ja5069323.; d) Pospíšil, L.; Bednárová, L.; Štěpánek, P.; Slavíček, P.; Vávra, J.; Hromadová, M.; Dlouhá, H.; Tarábek, J.;

Teplý, F. Intense Chiroptical Switching in a Dicationic Helicene-Like Derivative: Exploration of a Viologen-Type Redox Manifold of a Non-Racemic Helquat. *J. Am. Chem. Soc.* **2014**, *136* (31), 10826–10829. https://doi.org/10.1021/ja500220j.; e) Srebro, M.; Anger, E.; Moore II, B.; Vanthuyne, N.; Roussel, C.; Réau, R.; Autschbach, J.; Crassous, J. Ruthenium-Grafted Vinylhelicenes: Chiroptical Properties and Redox Switching. *Chem. - Eur. J.* **2015**, *21* (47), 17100–17115. https://doi.org/10.1002/chem.201502237.; f) Shen, C.; Loas, G.; Srebro-Hooper, M.; Vanthuyne, N.; Toupet, L.; Cador, O.; Paul, F.; López Navarrete, J. T.; Ramírez, F. J.; Nieto-Ortega, B.; Casado, J.; Autschbach, J.; Vallet, M.; Crassous, J. Iron Alkynyl Helicenes: Redox-Triggered Chiroptical Tuning in the IR and Near-IR Spectral Regions and Suitable for Telecommunications Applications. *Angew. Chem. Int. Ed.* **2016**, *55* (28), 8062–8066. https://doi.org/10.1002/anie.201601633.; g) Shen, C.; Srebro-Hooper, M.; Weymuth, T.; Krausbeck, F.; Navarrete, J. T. L.; Ramírez, F. J.; Nieto-Ortega, B.; Casado, J.; Reiher, M.; Autschbach, J.; Crassous, J. Redox-Active Chiroptical Switching in Mono- and Bis-Iron Ethynylcarbo[6]Helicenes Studied by Electronic and Vibrational Circular Dichroism and Resonance Raman Optical Activity. *Chem. - Eur. J.* **2018**, *24* (56), 15067–15079. https://doi.org/10.1002/chem.201803069.; h) Shen, C.; He, X.; Toupet, L.; Norel, L.; Rigaut, S.; Crassous, J. Dual Redox and Optical Control of Chiroptical Activity in Photochromic Dithienylethenes Decorated with Hexahelicene and Bis-Ethynyl-Ruthenium Units. *Organometallics* **2018**, *37* (5), 697–705. https://doi.org/10.1021/acs.organomet.7b00534.